

Our heads are round so our thoughts may change direction.

Francis Picabia (1879–1953).

Paradigms Lost.

Apologies to John Milton.

CHAPTER 21

The Meridional Overturning Circulation and the Antarctic Circumpolar Current

THE MERIDIONAL OVERTURNING CIRCULATION, or the MOC, of the ocean is the circulation associated with sinking mostly at high latitudes and upwelling elsewhere, with much of the meridional transport taking place below the main thermocline. Understanding this circulation is one of the main goals of this chapter. The theory explaining the MOC is not nearly as settled as that of the quasi-horizontal wind-driven circulation discussed in Chapter 19, but considerable progress has been made, in particular with a significant re-thinking of the fundamentals occurring in the late 20th and early 21st century, as we will discover. Our other main goal is to glean an understanding of the Antarctic Circumpolar Current, or ACC, the theory of which has also undergone a transformation over that same period. The ACC is important not only in its own right, but because it mediates the MOCs of the individual ocean basins, connecting them into a global circulation.

That there *is* a deep circulation has been known for a long time, largely from observations of tracers such as temperature, salinity, and constituents such as dissolved oxygen and silica.¹ We can also take advantage of numerical models that are able to assimilate observations (from hydrographic measurements, floats and satellites) and produce a state estimate of the overturning circulation that is consistent with both the observations and the equations of motion, and one such estimate is illustrated in Fig. 21.1. We see that the water does not all upwell in the subtropics as we tacitly assumed in the previous chapter. In fact, much of the mid-depth circulation more-or-less follows the isopycnals that span the two hemispheres (Fig. 21.2), sinking in the North Atlantic and upwelling in the Southern Ocean, with the transport in between being, at least in part, adiabatic.

The MOC used to be known as the ‘thermohaline’ circulation, reflecting the belief that it was primarily driven² by buoyancy forcing arising from gradients in temperature and salinity. Such a circulation requires that the diapycnal mixing must be sufficiently large, but many measurements have suggested this is not the case and that has led to a more recent view that the MOC is at least partially, and perhaps primarily, mechanically driven, mostly by winds, and so *along* isopycnals instead of across them. However, the situation is not wholly settled, and it is almost certain that both buoyancy and wind forcing, as well as diapycnal diffusion, all contribute. The possible role of multiple basins (Atlantic, Pacific, etc.) on the MOC is likewise not fully understood.

In the first half of the chapter we mainly discuss somewhat classical topics associated with the buoyancy forcing. Then, beginning in Section 21.6, we discuss the role of wind forcing in

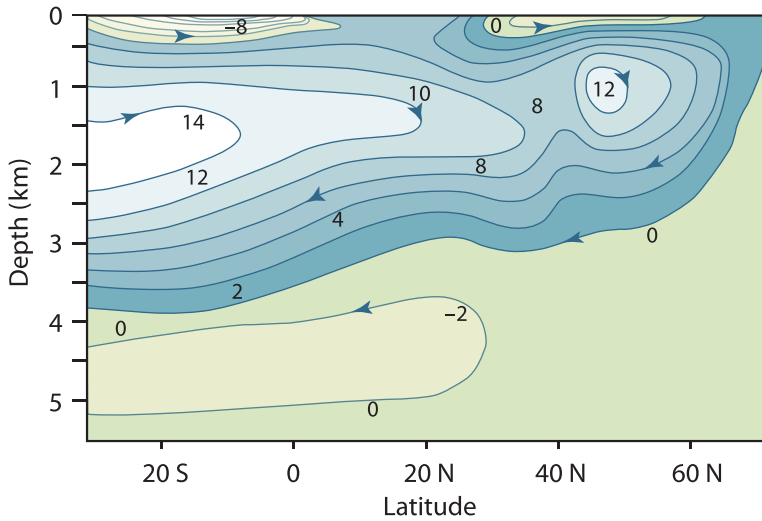


Fig. 21.1 An estimate of the mean meridional overturning circulation (i.e., the streamfunction of the zonally averaged meridional flow) in Sverdrups.³

producing a MOC. This forces us to take an extended diversion into the dynamics of the ACC in Section 21.7 and then, in the last two sections, we present a theory of the MOC that incorporates both wind and buoyancy effects. We start by considering a simple but revealing fluid model of buoyancy forcing at the surface in a very idealised setting.

21.1 SIDEWAYS CONVECTION

Perhaps the simplest and most obvious fluid dynamical model of the overturning circulation is that of *sideways convection*. The physical situation is sketched in Fig. 21.3. A fluid (two- or three-dimensional) is held in a container that is insulated on all of its sides and its bottom, but its upper surface is non-uniformly heated and cooled. In the purest fluid dynamical problem the heat enters the fluid solely by conduction at the upper surface, and one may suppose that here the temperature is imposed. Thus, for a simple Boussinesq fluid the equations of motion are

$$\frac{D\mathbf{v}}{Dt} + \mathbf{f} \times \mathbf{v} = -\nabla\phi + b\mathbf{k} + \nu\nabla^2\mathbf{v}, \quad \frac{Db}{Dt} = \kappa\nabla^2b, \quad \nabla \cdot \mathbf{v} = 0, \quad (21.1a,b,c)$$

where \mathbf{f} is the Coriolis parameter, and with boundary conditions

$$b(x, y, 0, t) = g(x, y), \quad (21.2)$$

where $g(x, y)$ is a specified field, and $\partial_n b = 0$ on the other boundaries, meaning that the derivative normal to the boundary, and so the buoyancy flux, is zero. The oceanographic relevance of (21.1) and (21.2) should be clear: the ocean is heated *and* cooled from above, and although the thermal forcing in the real ocean may differ in detail (being in part a radiative flux, and in part a sensible and latent heat transfer from the atmosphere), (21.2) is a useful idealization. An alternative upper boundary condition would be to impose a flux condition whereby

$$\text{flux} = \kappa \frac{\partial}{\partial z} b(x, y, 0, t) = h(x, y), \quad (21.3a)$$

where $h(x, y)$ is given. In some numerical models of the ocean, the heat input at the top is parameterized by way of a relaxation to some specified temperature. This is a form of flux condition in which

$$\kappa \frac{\partial b}{\partial z} = C(b^*(x, y) - b), \quad (21.3b)$$

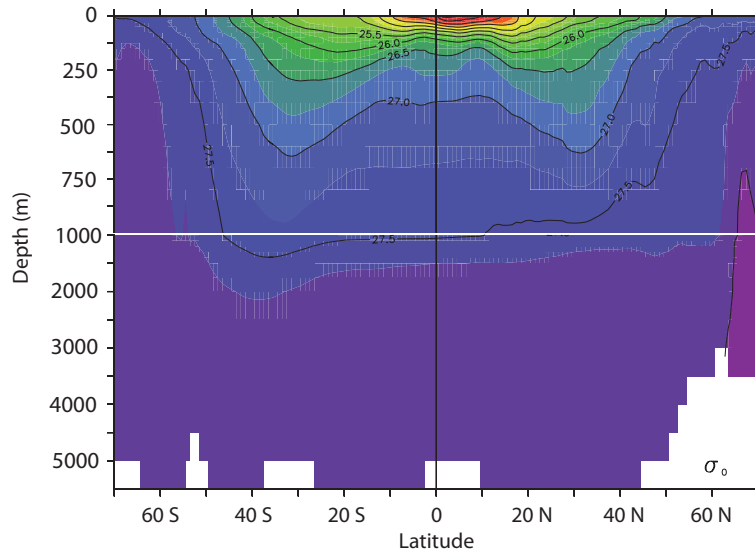


Fig. 21.2 The climatological zonally-averaged potential density (σ_0) in the Atlantic ocean. Note the break in the vertical scale at 1000 m. The region of rapid change of density (and temperature) is concentrated in the upper kilometre, in the main thermocline, below which the density is more uniform. The flow of the MOC is largely, but not exactly, parallel to the isopycnals.⁴

and C is an empirical constant and $b^*(x, y)$ is given.⁵ Although this may be a little more relevant than (21.2) for the real ocean, which of the three boundary conditions is chosen will not affect the arguments below, and we use (21.2).

21.1.1 Two-dimensional Convection

We may usefully restrict attention to the two-dimensional problem, in latitude and height. This is a poor model of the actual overturning circulation of the ocean, but the results do not depend on this idealization. The incompressibility of the flow then allows one to define a streamfunction such that

$$v = -\frac{\partial \psi}{\partial z}, \quad w = \frac{\partial \psi}{\partial y}, \quad \zeta = \nabla_x^2 \psi = \left(\frac{\partial^2 \psi}{\partial y^2} + \frac{\partial^2 \psi}{\partial z^2} \right), \quad (21.4)$$

where ζ is the vorticity in the meridional plane. We will omit the subscript x on the Laplacian operator where there is no ambiguity.

Taking the curl of Boussinesq equations of motion (21.1) then gives

$$\frac{\partial \nabla^2 \psi}{\partial t} + J(\psi, \nabla^2 \psi) = \frac{\partial b}{\partial y} + \nu \nabla^4 \psi, \quad (21.5a)$$

$$\frac{\partial b}{\partial t} + J(\psi, b) = \kappa \nabla^2 b, \quad (21.5b)$$

where $J(a, b) \equiv (\partial_y a)(\partial_z b) - (\partial_z a)(\partial_y b)$.

Nondimensionalization and scaling

We nondimensionalize (21.5) by formally setting

$$b = \Delta b \hat{b}, \quad \psi = \Psi \hat{\psi}, \quad y = L \hat{y}, \quad z = H \hat{z}, \quad t = \frac{LH}{\Psi} \hat{t}, \quad (21.6)$$

where the hatted variables are nondimensional, Δb is the temperature difference across the surface, L is the horizontal size of the domain, and Ψ , and ultimately the vertical scale H , are to be

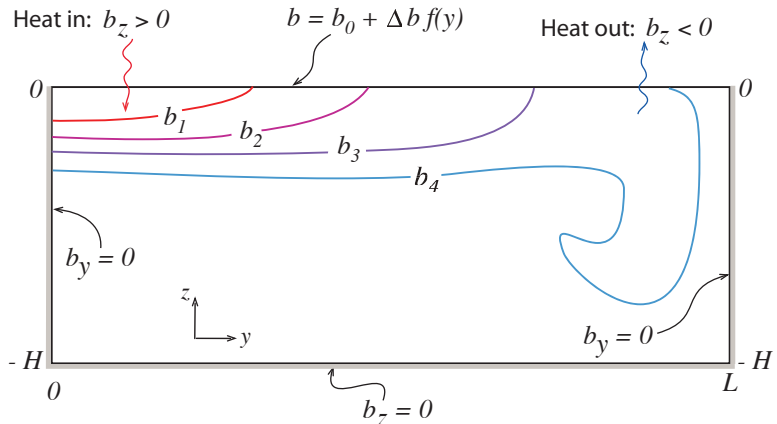


Fig. 21.3 Sketch of sideways convection. The fluid is differentially heated and cooled along its top surface, whereas all the other walls are insulating.

The result is, typically, a small region of convective instability and sinking near the coldest boundary, with generally upwards motion elsewhere.⁶

determined. Substituting (21.6) into (21.5) gives

$$\frac{\partial \hat{\nabla}^2 \hat{\psi}}{\partial \hat{t}} + \hat{J}(\hat{\psi}, \nabla^2 \hat{\psi}) = \frac{H^3 \Delta b}{\Psi^2} \frac{\partial \hat{b}}{\partial \hat{y}} + \frac{\nu L}{\Psi H} \hat{\nabla}^4 \hat{\psi}, \quad (21.7a)$$

$$\frac{\partial \hat{b}}{\partial \hat{t}} + \hat{J}(\hat{\psi}, \hat{b}) = \frac{\kappa L}{\Psi H} \hat{\nabla}^2 \hat{b}, \quad (21.7b)$$

where $\hat{\nabla}^2 = (H/L)^2 \partial^2 / \partial \hat{y}^2 + \partial^2 / \partial \hat{z}^2$ and the Jacobian operator is similarly nondimensional. If we now use (21.7b) to choose Ψ as

$$\Psi = \frac{\kappa L}{H}, \quad (21.8)$$

so that $t = H^2 \hat{t} / \kappa$, then (21.7) becomes

$$\frac{\partial \hat{\nabla}^2 \hat{\psi}}{\partial \hat{t}} + \hat{J}(\hat{\psi}, \hat{\nabla}^2 \hat{\psi}) = Ra \sigma \alpha^5 \frac{\partial \hat{b}}{\partial \hat{y}} + \sigma \hat{\nabla}^4 \hat{\psi}, \quad (21.9)$$

$$\frac{\partial \hat{b}}{\partial \hat{t}} + \hat{J}(\hat{\psi}, \hat{b}) = \hat{\nabla}^2 \hat{b}. \quad (21.10)$$

It is possible to make different scaling choices, but they all lead to the appearance of the same non dimensional parameters, or combinations thereof, and the three that govern the behaviour of the system are

$$Ra = \left(\frac{\Delta b L^3}{\nu \kappa} \right), \quad (\text{the Rayleigh number}), \quad (21.11a)$$

$$\sigma = \frac{\nu}{\kappa}, \quad (\text{the Prandtl number}), \quad (21.11b)$$

$$\alpha = \frac{H}{L}, \quad (\text{the aspect ratio}). \quad (21.11c)$$

Sometimes H is used instead of L in the Rayleigh number definition; we use L here because it is an external parameter. The Rayleigh number is a measure of the strength of the buoyancy forcing relative to the viscous term, and in the ocean it will be very large indeed, perhaps $\sim 10^{24}$ if molecular values are used.

For steady non-turbulent flows, and also perhaps for statistically steady flows, we can demand that the buoyancy term in (21.9) is $\mathcal{O}(1)$. If it is smaller then the flow is not buoyancy driven, and

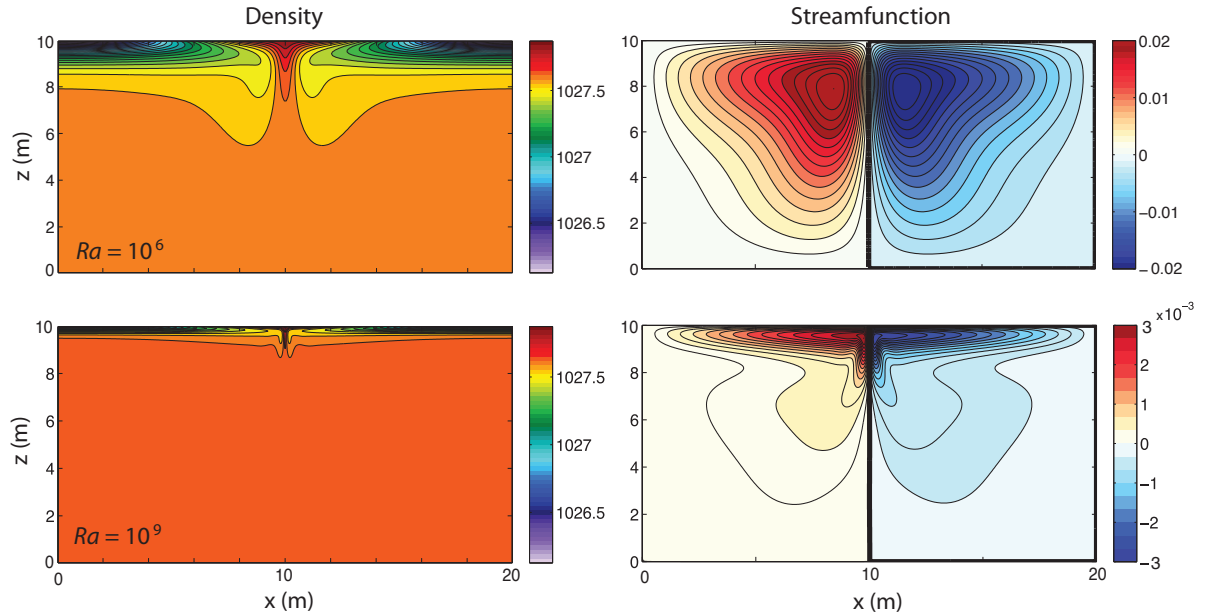


Fig. 21.4 The density and streamfunction in two numerical simulations of two-dimensional sideways convection, with Rayleigh numbers of 10^6 (top) and 10^9 (bottom). The imposed temperature at the top linearly decreases from the centre outward, the side and bottom walls are insulating, and the Prandtl number is 10. The two density plots use the same colourmap, but the streamfunction plots do not. There is a sinking plume at the centre, with a weaker circulation and a thinner thermocline at the higher Rayleigh number.⁸

if it is larger there is nothing to balance it. Our demand can be satisfied only if the vertical scale of the motion adjusts appropriately and, for $\sigma = \mathcal{O}(1)$, this suggests the scalings:⁷

$$H = L\sigma^{-1/5}Ra^{-1/5} = \left(\frac{\kappa^2 L^2}{\Delta b} \right)^{1/5}, \quad \Psi = Ra^{1/5}\sigma^{-4/5}\nu = (\kappa^3 L^3 \Delta b)^{1/5}. \quad (21.12a,b)$$

The vertical scale H arises as a consequence of the analysis, and the vertical size of the domain plays no direct role. [For $\sigma \gg 1$ we might expect the nonlinear terms to be small and if the buoyancy term balances the viscous term in (21.9) the right-hand sides of (21.12) are multiplied by $\sigma^{1/5}$ and $\sigma^{-1/5}$. For seawater, $\sigma \approx 7$ using the molecular values of κ and ν . If small scale turbulence exists, then the eddy viscosity will likely be similar to the eddy diffusivity and $\sigma \approx 1$.] Numerical experiments (an example is shown in Fig. 21.4) provide support for the scaling of (21.12), and a few simple and robust points that have relevance to the real ocean emerge:

- Most of the box fills up with the densest available fluid, with a boundary layer in temperature near the surface required in order to satisfy the top boundary condition. The boundary gets thinner with decreasing diffusivity, consistent with (21.12). This is a diffusive prototype of the oceanic thermocline.
- The horizontal scale of the overturning circulation is large, nearly the scale of the box.
- The downwelling regions (the regions of convection) are of smaller horizontal scale than the upwelling regions, especially as the Rayleigh number increases.

Let us now try to explain some of the features in a simple and heuristic way, beginning with the scale of the motion.

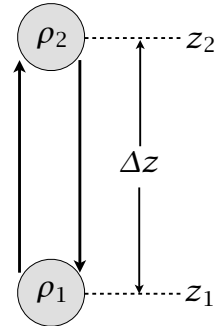


Fig. 21.5 Two fluid parcels, of density ρ_1 and ρ_2 and initially at positions z_1 and z_2 respectively, are interchanged. If $\rho_2 > \rho_1$ then the final potential energy is lower than the initial potential energy, with the difference being converted into kinetic energy.

21.1.2 The Relative Scale of Convective Plumes and Diffusive Upwelling

Why is the downwelling region narrower than the upwelling? The short answer is that high Rayleigh number convection is much more efficient than diffusive upwelling, so that the convective buoyancy flux can match the diffusive flux only if the convective plumes cover a much smaller area than diffusion.⁹ Suppose that the basin is initially filled with water of an intermediate temperature, and that surface boundary conditions of a temperature decreasing linearly from low latitudes to high latitudes are imposed. The deep water will be convectively unstable, and convection at high latitudes (where the surface is coldest) will occur, quickly filling the abyss with dense water. After this initial adjustment the deep, dense water at lower latitudes will be slowly warmed by diffusion, but at the same time surface forcing will maintain a cold high latitude surface, thus leading to high latitude convection. A steady state or statistically steady state is eventually reached with the deep water having a slightly lower potential density than the surface water at the highest latitudes, and so maintaining continual convection, but convection that takes place only at the highest latitudes.

To see this more quantitatively consider the respective efficiencies of the convective heat flux and the diffusive heat flux. Consider an idealized re-arrangement of two parcels, initially with the heavier one on top as illustrated in Fig. 21.5. The potential energy released by the re-arrangement, ΔP is given by

$$\Delta P = P_{\text{final}} - P_{\text{initial}} \quad (21.13)$$

$$= g [(\rho_1 z_2 + \rho_2 z_1) - (\rho_1 z_1 + \rho_2 z_2)] \quad (21.14)$$

$$= g(z_2 - z_1)(\rho_1 - \rho_2) = \rho_0 \Delta b \Delta z, \quad (21.15)$$

where $\Delta z = z_2 - z_1$ and $\Delta b = g(\rho_1 - \rho_2)/\rho_0$.

The kinetic energy gained by this re-arrangement, ΔK is given by $\Delta K = \rho_0 w^2$ and equating this to (21.13) gives

$$w^2 = -\Delta b \Delta z. \quad (21.16)$$

If the heavier fluid is initially on top then $\rho_2 > \rho_1$ and, as defined, $\Delta b < 0$. The vertical convective buoyancy flux per unit area, B_c , is given by $B_c = w \Delta b$ and using (21.16) we find

$$B_c = (-\Delta b)^{3/2} (\Delta z)^{1/2}. \quad (21.17)$$

The upwards diffusive flux, B_d , per unit area is given by

$$B_d = \kappa \frac{\Delta b}{H}, \quad (21.18)$$

where H is the thickness of the layer over which the flux occurs. In a steady state the total diffusive flux must equal the convective flux so that, from (21.17) and (21.18),

$$(-\Delta b)^{3/2} (\Delta z)^{1/2} \delta = \kappa \frac{\Delta b}{H}, \quad (21.19)$$

where δ is the fractional area over which convection occurs. If we set $\Delta z = H$, and use (21.12a) we find

$$(-\Delta b)^{3/2} \left(\frac{\kappa^2 L^2}{\Delta b} \right)^{1/10} \delta = \kappa \frac{\Delta b}{(\kappa^2 L^2 / \Delta b)^{1/5}}, \quad (21.20)$$

giving

$$\delta = \left(\frac{\kappa^2}{\Delta b L^3} \right)^{1/5} = (Ra \sigma)^{-1/5}. \quad (21.21)$$

For geophysically relevant situations this is a very small number, usually smaller than 10^{-5} . Although the details of the above calculation may be questioned (for example, the use of the same buoyancy difference and vertical scale in the convection and the diffusion), the physical basis for the result is transcendent: for realistic choices of the diffusivity the convection is much more efficient than the diffusion and so will occur over a much smaller area.

21.1.3 Phenomenology of the Overturning Circulation

No water can be denser (or, more accurately, have a greater potential density) than the densest water at the surface. If the surface water is denser than the water at depth then it will be convectively unstable and sink in a plume.¹⁰ The plume slowly entrains the warmer water that surrounds it, and then spreads horizontally when it reaches the bottom or when its density becomes similar to that of its surroundings. The presence of water denser than its surroundings creates a horizontal pressure gradient, and the ensuing flow will displace any adjacent lighter fluid, and so the domain fills with the densest available fluid. This process is a continuous one: the plumes take cold water into the interior, where the water slowly warms by diffusion, and the source of cold water at the surface is continuously replenished. If diffusion is small, the end result is that the potential density of the fluid in the interior will be slightly less than that of the densest fluid formed at the surface. (Because diffusion can act only to reduce extrema, no fluid in the interior can be colder than the coldest fluid formed at the surface.)

However, the value at the surface is given by the boundary condition $b(x, y, z = 0) = f(x, y)$. Thus, the interior cannot fill all the way to the surface with this cold water and there must be a boundary layer connecting the cold, dense interior with the surface; its thickness δ is given by the height scale of (21.12a); that is $\delta \sim H = (\kappa^2 L^2 / \Delta b)^{1/5}$. Such a strong boundary layer will not necessarily be manifest in the velocity field, however, because the no-normal flow boundary condition on the velocity field is satisfied by setting $\psi = 0$ as a boundary condition to the elliptic problem $\nabla^2 \psi = \zeta$, where ζ is the prognostic variable in (21.5a), and this boundary condition has a global effect on the velocity field.

Why is the horizontal scale of the circulation large? The circulation transfers heat meridionally, and it is far more efficient to do this by a single overturning cell than by a multitude of small cells; hence, although we cannot entirely eliminate the possibility that some instability will produce such small scales of motion, it seems likely the horizontal scale of the mean circulation will be determined by the domain scale. (At low Rayleigh number we can in fact explicitly calculate an approximate analytic solution for the flow, demonstrating this.) For higher Rayleigh number perturbation approaches fail and we must resort to numerical solutions; these (e.g., Fig. 21.4), do show the circulation dominated by a single overturning circulation rather than many small convective cells over a large range of Rayleigh number.

Finally, it is important to realize that *even for large diffusion and viscosity there is no stationary solution*: as soon as we impose a temperature gradient at the top the fluid begins to circulate, a manifestation of the dictum that a baroclinic fluid is a moving fluid, encountered in Section 4.2. Put simply, a temperature gradient leads a density gradient, which in turn leads to a pressure gradient.

The pressure gradient leads to motion: viscosity cannot prevent that, for it can have an effect only if the velocity is non-zero.

21.2 THE MAINTENANCE OF SIDEWAYS CONVECTION

In most conventional convection problems the fluid is heated from below, becomes buoyant and rises, and is cooled at the top. In contrast, in sideways convection the heating and cooling occur at the same level, and the conditions under which a circulation can be maintained are by no means clear; our purpose here is to make them clearer. The energetic derivations of this section are but an extension of Section 2.4.3, but now with starring roles for friction, diffusion and the boundary conditions, and the reader may wish to review that section first. The derivations below are not difficult, but they lead to powerful and perhaps counter-intuitive results that provide important information about the overturning circulation of the real ocean. To begin, we rewrite the equations of motion, (21.1), in a slightly different way, namely

$$\frac{\partial \mathbf{v}}{\partial t} + (\mathbf{f} + 2\boldsymbol{\omega}) \times \mathbf{v} = -\nabla B + b\mathbf{k} + \nu\nabla^2\mathbf{v}, \quad (21.22a)$$

$$\frac{\partial b}{\partial t} + \nabla \cdot (\mathbf{b}\mathbf{v}) = \dot{Q} = J + \kappa\nabla^2 b, \quad (21.22b)$$

$$\nabla \cdot \mathbf{v} = 0, \quad (21.22c)$$

where $B = \mathbf{v}^2/2 + \phi$ is the Bernoulli function for Boussinesq flow and \dot{Q} ($= \dot{b}$) is the total rate of heating (including diffusion, and absorbing constant factors such as heat capacity into its definition) with J its non-diffusive component. The fluid occupies a finite volume, and in a steady state $\langle \dot{Q} \rangle = 0$, where the angle brackets denote a volume and time integration.

21.2.1 The Energy Budget

To obtain an energy budget we follow the procedure of Section 2.4.3. First take the dot product of (21.22a) with \mathbf{v} to give

$$\frac{1}{2} \frac{\partial \mathbf{v}^2}{\partial t} = -\nabla \cdot (\mathbf{v}B) + wb + \nu\mathbf{v} \cdot \nabla^2\mathbf{v}. \quad (21.23)$$

Integrating over a domain bounded by stress-free rigid walls gives the kinetic energy equation

$$\frac{d}{dt} \left\langle \frac{1}{2} \mathbf{v}^2 \right\rangle = \langle wb \rangle - \varepsilon, \quad (21.24)$$

where angle brackets denote (for the moment) just a volume average and ε is the average dissipation of kinetic energy ($\varepsilon = -\nu \langle \mathbf{v} \cdot \nabla^2 \mathbf{v} \rangle = \nu \langle \boldsymbol{\omega}^2 \rangle$), a positive definite quantity. Thus, in a statistically steady state in which the left-hand side vanishes after time averaging, the dissipation of kinetic energy is maintained by the buoyancy flux; that is, by a release of potential energy with light fluid ascending and dense fluid descending.

We obtain a potential energy budget by using (21.22b) to write

$$\frac{Dbz}{Dt} = z \frac{Db}{Dt} + b \frac{Dz}{Dt} = z\dot{Q} + bw, \quad (21.25)$$

and integrating this over the domain gives the potential energy equation

$$\frac{d}{dt} \langle bz \rangle = \langle z\dot{Q} \rangle + \langle bw \rangle. \quad (21.26)$$

Subtracting (21.26) from (21.24) gives the energy equation

$$\frac{d}{dt} \left\langle \frac{1}{2} \mathbf{v}^2 - bz \right\rangle = -\langle z\dot{Q} \rangle - \varepsilon. \quad (21.27)$$

21.2.2 Conditions for Maintaining a Thermally-driven Circulation

In a statistically steady state the left-hand side of (21.27) vanishes and the kinetic energy dissipation is balanced by the buoyancy source terms; that is

$$\langle z\dot{Q} \rangle = -\varepsilon < 0. \quad (21.28)$$

The right-hand side (the term $-\varepsilon$) is negative definite, and to balance this the heating must be negatively correlated with height. (Recall that $\langle \dot{Q} \rangle = 0$, and the origin of the z -coordinate is then immaterial.) Thus, *in order to maintain a circulation in which kinetic energy is dissipated, the heating (including diffusive heating) must occur, on average, at lower levels than the cooling.* This result is related to, but not quite the same as, a postulate due to Sandström, discussed below.

In the ocean the non-diffusive heating occurs predominantly at the surface, except for the negligible effects of hydrothermal vents. Thus, $\langle J_z \rangle \approx 0$ and a kinetic-energy-dissipating circulation can *only* be maintained, in the absence of mechanical forcing, if the diffusion is non-zero — in that case heat may be diffused from the surface to depth, so effectively providing a deep heat source. In the atmosphere, the heating is mostly at the surface and cooling is mostly in the mid-troposphere so that $\langle z\dot{Q} \rangle < 0$; thus, (21.28) is readily satisfied and the circulation is not restricted.

♦ *Maintaining a steady baroclinic circulation*

By a rather different method — and one closer to a suggestion of Sandström dating from 1908 — we can obtain a result that is different from but related to (21.28).¹¹ Using (4.37) and (21.22a), the circulation in a Boussinesq system obeys

$$C = \oint \mathbf{v} \cdot d\mathbf{r}, \quad \frac{DC}{Dt} = \oint b\mathbf{k} \cdot d\mathbf{r} + \oint \mathbf{F} \cdot d\mathbf{r}, \quad (21.29a,b)$$

where C is the circulation, $d\mathbf{r}$ is a path element, and \mathbf{F} represents the frictional terms. (The Coriolis parameter plays no role in this argument because the Coriolis force does no work, and f may be set to zero without loss of generality.) Now we may write the rate of change of circulation in the form

$$\frac{DC}{Dt} = \oint \left(\frac{\partial \mathbf{v}}{\partial t} + \mathbf{v} \cdot \nabla \mathbf{v} \right) \cdot d\mathbf{r} = \oint \left(\frac{\partial \mathbf{v}}{\partial t} + \boldsymbol{\omega} \times \mathbf{v} \right) \cdot d\mathbf{r}, \quad (21.30)$$

because the integral of the potential term that arises when going to the last expression vanishes. Let us assume the flow is steady, so that $\partial \mathbf{v} / \partial t$ vanishes. Let us further choose the path of integration to be a streamline, which since the flow is steady is also a parcel trajectory. The second term on the right-most expression of (21.30) then also vanishes and (21.29b) becomes

$$\oint b dz = - \oint \mathbf{F} \cdot d\mathbf{r} = - \oint \frac{\mathbf{F}}{|\mathbf{v}|} \cdot \mathbf{v} dr, \quad (21.31)$$

where the last equality follows because the path is everywhere parallel to the velocity. Let us now assume that the friction retards the flow, and that $\oint \mathbf{F} \cdot \mathbf{v} / |\mathbf{v}| dr < 0$. (One form of friction that has this property is linear drag, $\mathbf{F} = -C\mathbf{v}$ where C is a constant. The property is similar to, but not the same as, the property that the friction dissipates kinetic energy over the circuit.) Making this assumption, if we integrate the term on the left-hand side by parts we obtain

$$\oint z db < 0. \quad (21.32)$$

Now, because the integration circuit in (21.32) is a fluid trajectory, the change in buoyancy db is proportional to the heating of a fluid element as it travels the circuit; in the notation of (21.22b),

$db = \dot{Q} dt$, where the heating, \dot{Q} , includes diffusive effects. Thus, the inequality implies that the net heating must be negatively correlated with height: that is, *the heating must occur, on average, at a lower level than the cooling in order that a steady circulation may be maintained against the retarding effects of friction.*

A similar result can be obtained for a compressible fluid. From Equations (4.43)–(4.45) on page 151 we write the baroclinic circulation theorem as

$$\frac{DC}{Dt} = \oint p d\alpha + \oint F \cdot dr = \oint T d\eta + \oint F \cdot dr, \quad (21.33)$$

where η is the specific entropy. Then, by precisely the same arguments as led to (21.32), we are led to the requirements that

$$\oint T d\eta > 0 \quad \text{or equivalently} \quad \oint p d\alpha > 0. \quad (21.34a,b)$$

Equation (21.34a) means that parcels must gain entropy at high temperatures and lose entropy at low temperatures; similarly, from (21.32b), a parcel must expand ($d\alpha > 0$) at high pressures and contract at low pressures.

For an ideal gas we can put these statements into a form analogous to (21.32) by noting that $d\eta = c_p(d\theta/\theta)$, where θ is potential temperature, and using the definition of potential temperature, (1.105). With these we have

$$\oint T d\eta = \oint c_p \frac{T}{\theta} d\theta = \oint c_p \left(\frac{p}{p_R} \right)^\kappa d\theta, \quad (21.35)$$

and (21.34a) becomes

$$\oint c_p \left(\frac{p}{p_R} \right)^\kappa d\theta > 0. \quad (21.36)$$

Because the path of integration is a fluid trajectory, $d\theta$ is proportional to the heating of a fluid element. Thus, as with the Boussinesq result, (21.36) implies that *the heating (the potential temperature increase) must occur at a higher pressure than the cooling in order that a steady circulation may be maintained against the retarding effects of friction.*

These results may be understood by noting that the heating must occur at a higher pressure than the cooling in order that work may be done, the work being necessary to convert potential energy into kinetic energy to maintain a circulation against friction. Intuitively, if the heating is below the cooling, then the heated fluid will expand and become buoyant and rise, and a steady circulation between heat source and heat sink can readily be imagined. On the other hand, if the heating is above the cooling there is no obvious pathway between source and sink.

Intuitive as these results may be, the conditions required to prove (21.32) and (21.36) are much more restrictive than those needed to prove (21.28). To prove the former, we must *assume* that the flow is absolutely steady, *and* that streamlines form a closed path, *and* that the friction has retarding properties. The second of these conditions is not generally satisfied in three dimensions, even when the flow is steady. Furthermore, one cannot prove that Newtonian viscosity ($\nu \nabla^2 \mathbf{v}$) will always act to retard the flow. On the other hand, (21.28) provides a condition for the maintenance of a statistically steady circulation, assuming only that the friction acts to dissipate kinetic energy. In any case, it is clear from all of the above results that the overturning circulation is greatly affected by the relative pressures at the locations of the heating and cooling, and this is called *Sandström's effect*. In all of these cases, the heating must be taken to include diffusive effects; if the molecular diffusivity is small and the heating is at the surface we can further constrain the flow, as we now see.

21.2.3 Surface Fluxes and Non-turbulent Flow at Small Diffusivities

Suppose that the only heating to the fluid is via diffusion through the upper surface; that is $J = 0$ in (21.22b). Is a circulation possible? If the diffusivity is finite then heat can diffuse into the fluid and thereby potentially provide a difference in altitude between the heating and the cooling. However, as $\kappa \rightarrow 0$ this mechanism ceases to operate and we therefore expect that the left-hand sides of (21.28) and (21.32) will go to zero, and the circulation will cease. In what follows we put this argument on a more rigorous footing: we will show that as $\kappa \rightarrow 0$ the kinetic energy dissipation also goes to zero, and therefore the flow is ‘non-turbulent’, the meaning of which will be made clearer below.

Assuming a statistically steady state, integrating (21.22b) horizontally gives

$$\frac{\partial \overline{bw}}{\partial z} = \kappa \frac{\partial^2 \bar{b}}{\partial z^2}, \quad (21.37)$$

where an overbar indicates a horizontal average. Integrating this equation up from the bottom (where there is no flux) to a level z gives

$$\overline{wb} - \kappa \bar{b}_z = 0 \quad (21.38)$$

at every level in the fluid. The two terms on the left-hand side together give rise to the total buoyancy flux through the level z , and the flux must vanish because there is no buoyancy input except at the surface. If we integrate this vertically we have

$$\langle wb \rangle = H^{-1} \kappa [\bar{b}(0) - \bar{b}(-H)], \quad (21.39)$$

where the angle brackets denote an average over the entire volume. In the limit $\kappa \rightarrow 0$, the integrated advective buoyancy flux will vanish, because the term $\bar{b}(0) - \bar{b}(-H)$ remains finite. This follows because b is conserved on parcels, except for the effects of diffusion, which can only act to reduce the value of extrema in the fluid. Thus, $\bar{b}(0) - \bar{b}(-H)$ can only be as large as the temperature difference at the surface, which is set by the boundary conditions.

Now consider the kinetic energy budget. Using (21.24) and (21.39) we have in a statistically steady state

$$\varepsilon = H^{-1} \kappa [\bar{b}(0) - \bar{b}(-H)]. \quad (21.40)$$

Because, as noted above, the buoyancy difference on the right-hand side is bounded, the kinetic energy dissipation must go to zero if the thermal diffusivity goes to zero; that is, $\varepsilon \rightarrow 0$ as $\kappa \rightarrow 0$ and in particular $\varepsilon < \kappa \Delta b / H$ where Δb is the maximum buoyancy difference at the surface. We may also consider the limit $(\kappa, \nu) \rightarrow 0$ with a fixed Prandtl number, $\sigma \equiv \nu/\kappa$, and in this limit the energy dissipation also vanishes with κ .

Finally, let us see how the surface buoyancy is related to the buoyancy flux, for any value of κ . Multiplying (21.22b) (with $J = 0$) by b and integrating over the domain gives the buoyancy variance equation

$$\frac{1}{2} \frac{d \langle b^2 \rangle}{dt} = \kappa \left[b \frac{\partial \bar{b}}{\partial z} \Big|_{z=0} - \langle |\nabla b|^2 \rangle \right]. \quad (21.41)$$

We have assumed that the normal derivative of b vanishes on all surfaces except the top one ($z = 0$) and an overbar denotes a horizontal average. In a statistically steady state,

$$\overline{b \frac{\partial \bar{b}}{\partial z}} \Big|_{z=0} = \langle |\nabla b|^2 \rangle, \quad (21.42)$$

where the overbar and angle brackets now also imply a time average. The right-hand side is positive definite, and thus there must be a positive correlation between b and $\partial b/\partial z$, meaning that there is a heat flux into the fluid where it is hot, and a heat flux out of the fluid where it is cold. This result holds no matter whether the upper boundary condition is a condition on b or on $\partial b/\partial z$.

Interpretation

The result encapsulated by (21.40) means that, for a fluid forced only at the surface by buoyancy forcing, as the diffusivity goes to zero so does the energy dissipation. For a fluid of finite viscosity the vorticity in the fluid must then go to zero, because $\varepsilon = \nu \langle \omega^2 \rangle$; this in turn means that the flow cannot be baroclinic, because baroclinicity generates vorticity, even in the presence of viscosity (Section 4.2). An even more interesting result follows for a fluid with small viscosity. In turbulent flow, the energy dissipation at high Reynolds number is not a function of the viscosity; if the viscosity is reduced, the cascade of energy to smaller scales merely continues to still smaller scale, generating vorticity at these smaller scales, and the energy dissipation is unaltered, remaining finite even in the limit $\nu \rightarrow 0$. In contrast, for a fluid heated and cooled only at the upper surface, the energy dissipation *tends to zero* as $\kappa \rightarrow 0$, whether or not one is in the high-Reynolds number limit. This means that vorticity cannot be generated at the viscous scales by the action of a turbulent cascade, as that would lead to energy dissipation. Effectively, the result prohibits an ocean that is forced only at the surface by a buoyancy flux from having an ‘eddy viscosity’ that would enable the fluid to efficiently dissipate energy, and if there is no small scale motion producing an eddy viscosity there can be no eddy diffusivity either. Thus, such an ocean is *non-turbulent*. This is a rather different picture from that of the real ocean, where there is some dissipation of energy in the interior because of breaking gravity waves, and dissipation at the boundary in Ekman layers, and the eddy diffusivity is needed for there to be a non-negligible buoyancy-driven meridional overturning circulation.

Of course, thermal forcing in the ocean is in part an imposed flux, coming from radiation among other things, and this penetrates below the surface. However, this makes little physical difference to the argument, provided that this forcing remains confined to the upper ocean. If so, then for any level below this forcing we still have the result (21.38), and the final result (21.40) holds, assuming that the range of temperatures produced by the forcing is still finite.

21.2.4 The Importance of Mechanical Forcing

The results of (21.28) and (21.40) do not, strictly speaking, prohibit there from being a thermal circulation, with fluid sinking at high latitudes and rising at low, even for zero diffusivity. However, in the absence of any mechanical forcing, this circulation must be laminar, even at high Rayleigh number, meaning that flow is not allowed to break in such a way that energy can be dissipated — a very severe constraint that most flows cannot satisfy. The scalings (21.12) further suggest that the magnitude of the circulation in fact scales (albeit nonlinearly) with the size of the molecular diffusivity, and if these scalings are correct the circulation will in fact diminish as $\kappa \rightarrow 0$. For small diffusivity, the solution most likely to be adopted by the fluid is for the flow to become confined to a very thin layer at the surface, with no abyssal motion at all, which is completely unrealistic vis-à-vis the observed ocean. Thus, the deep circulation of the ocean cannot be considered to be wholly forced by buoyancy gradients at the surface.

Suppose we add a mechanical forcing, F , to the right-hand side of (21.22a); this might represent wind forcing at the surface, or tides. The kinetic energy budget becomes

$$\varepsilon = \langle wb \rangle + \langle F \cdot v \rangle = H^{-1} \kappa [\bar{b}(0) - \bar{b}(-H)] + \langle F \cdot v \rangle. \quad (21.43)$$

In this case, even for $\kappa = 0$, there is a source of energy and therefore turbulence (i.e., a dissipative circulation) can be maintained. The turbulent motion at small scales then provides a mechanism of mixing and so can effectively generate an ‘eddy diffusivity’ of buoyancy. *Given* such an eddy

diffusivity, wind forcing is no longer necessary for there to be an overturning circulation. Therefore, it is useful to think of mechanical forcing as having two distinct effects:

- (i) The wind provides a stress on the surface that may directly drive the large-scale circulation, including the overturning circulation. (An example of this is discussed in Section 21.6.)
- (ii) Both tides and the wind provide a mechanical source of energy to the system that allows the flow to become turbulent and so provides a source for an eddy diffusivity and eddy viscosity.

In either case, we may conclude that the presence of mechanical forcing is necessary for there to be an overturning circulation in the world's oceans of the kind observed. Let us first suppose that the most important effect of the wind is that it enables there to be an eddy diffusivity that is much larger than the molecular one; the eddy diffusivity enables large volumes of the ocean to become mixed, so allowing a buoyancy-driven overturning circulation (a 'thermohaline circulation') to exist.

21.2.5 The Mixing-driven Ocean

Before moving on to other matters, let's make a connection to the scaling for the overturning circulation discussed in Section 20.5.1. In that section we considered the planetary-geostrophic equations,

$$\mathbf{v} \cdot \nabla b = \kappa \nabla^2 b, \quad \nabla \cdot \mathbf{u} + \frac{\partial w}{\partial z} = 0, \quad \mathbf{f} \times \mathbf{u} = -\nabla \phi, \quad b = \frac{\partial \phi}{\partial z}, \quad (21.44a,b,c,d)$$

and obtained, after a little algebra, the scalings for vertical velocity and thermocline thickness,

$$W = \kappa^{2/3} \left(\frac{\beta \Delta b}{f^2 L} \right)^{1/3}, \quad \delta = \kappa^{1/3} \left(\frac{f^2 L}{\beta \Delta b} \right)^{1/3}. \quad (21.45)$$

These are different in detail from the Rossby scalings, (21.12), but they also require a finite diffusivity to produce a circulation and a thermocline. The Sandström effect applies, as it must, to oceanically relevant equations.

In order for the scales given in (21.45) to be representative of those observed in the real ocean, we must use an eddy diffusivity for κ . Using $f = 10^{-4} \text{ s}^{-1}$, $\beta = 10^{-11} \text{ m}^{-1} \text{ s}^{-1}$, $L = 5 \times 10^6 \text{ m}$, $g = 10 \text{ m s}^{-2}$, $\kappa = 10^{-5} \text{ m}^2 \text{ s}^{-1}$, $\Delta b = -g\Delta\rho/\rho_0 = g\beta_T\Delta T$ and $\Delta T = 10 \text{ K}$ we find the not unreasonable values of $\delta \approx 150 \text{ m}$ and $W = 10^{-7} \text{ m s}^{-1}$, albeit δ is rather smaller than the thickness of the observed thermocline. However, if we take the molecular value of $\kappa \approx 10^{-7} \text{ m}^2$ the values of W and δ are unrealistically small (although still non-zero). Evidently, if the deep circulation of the ocean is buoyancy (or mixing) driven, it must take advantage of turbulence that enhances the small scale mixing and produces an eddy diffusivity.

21.3 ♦ SIMPLE BOX MODELS

This section is marked with a black diamond not because it is advanced; rather, it is a little peripheral to our main development. The purist may consider this section a diversion away from a consideration of the fluid dynamical properties of the ocean, and the content implied by the title of this book, but such box models have been quite fecund and an evident source of qualitative understanding, and thus find a place in our discussion, if not in our canon. Readers may skim this section without fear of disapprobation.

Even though they are far simpler than the real ocean, the fluid dynamical models of the previous sections are still quite daunting. The analysis that can be performed is either very specific and of little generality, for example the construction of solutions at low Rayleigh number, or it is a very general form such as scaling or energetic arguments. Models based on the fluid dynamical equations do not easily allow for the construction of explicit solutions in the parameter regime — high

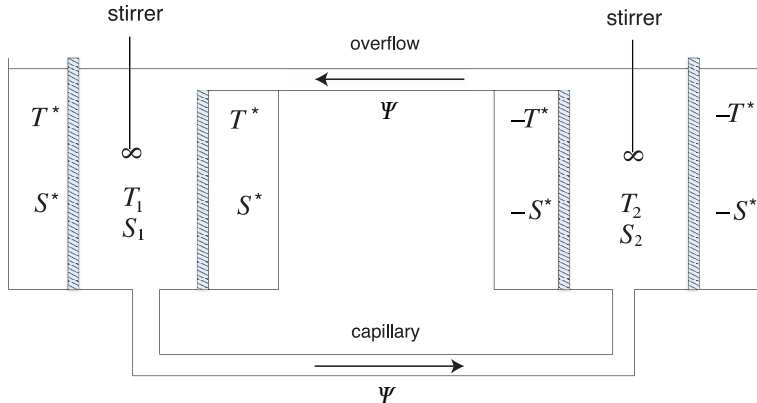


Fig. 21.6 A two-box model of the overturning circulation of the ocean. The shaded walls are porous, and each box is well mixed by its stirrer. Temperature and salinity evolve by way of fluid exchange between the boxes via the capillary tube and the overflow, and by way of relaxation with the two infinite reservoirs at $(+T^*, +S^*)$ and $(-T^*, -S^*)$.

Rayleigh and Reynolds numbers — of interest. It is therefore useful to consider an extreme simplification of the overturning circulation, namely *box models*. These are caricatures of the circulation, constructed by dividing the ocean into a small number of boxes with simple rules determining the transport of fluid properties between them.¹²

21.3.1 A Two-box Model

Consider two boxes as illustrated in Fig. 21.6. Each box is well-mixed and has a uniform temperature and salinity, T_1, T_2 and S_1, S_2 . The boxes are connected with a capillary tube at the bottom along which the flow is viscous, obeying Stokes' Law. That is, the flow along the tube is proportional to the pressure gradient which, because the flow is hydrostatic, is proportional to the density difference between the two boxes. An overflow at the top keeps the upper surfaces of the two boxes at the same level. Thus, the circulation, Ψ , is given by

$$\Psi = A(\rho_1 - \rho_2), \quad (21.46)$$

where ρ_1 and ρ_2 are the densities of the fluids in the two boxes and A is a constant. The boxes are enclosed by porous walls beyond which are reservoirs of constant temperature and salinity, and we are at liberty to choose the origin of the temperature scale such that the two reservoirs are at $+T^*$ and $-T^*$, and similarly for salinity. Thus, heat and salt are transferred into and out of the boxes as represented by simple linear laws and we have

$$\begin{aligned} \frac{dT_1}{dt} &= c(T^* - T_1) - |\Psi|(T_1 - T_2), & \frac{dT_2}{dt} &= c(-T^* - T_2) - |\Psi|(T_2 - T_1), \\ \frac{dS_1}{dt} &= d(S^* - S_1) - |\Psi|(S_1 - S_2), & \frac{dS_2}{dt} &= d(-S^* - S_2) - |\Psi|(S_2 - S_1). \end{aligned} \quad (21.47)$$

The advective transfer is independent of the sign of the circulation, because it occurs through both the capillary tube and the overflow. From these equations it is easy to show that the sum of the temperatures, $T_1 + T_2$ decays to zero and is uncoupled from the difference, and similarly for salinity. Defining $\hat{T} = (T_1 - T_2)/(2T^*)$ and $\hat{S} = (S_1 - S_2)/(2S^*)$, we obtain

$$\frac{d\hat{T}}{dt} = c(1 - \hat{T}) - 2|\Psi|\hat{T}, \quad \frac{d\hat{S}}{dt} = d(1 - \hat{S}) - 2|\Psi|\hat{S}. \quad (21.48a,b)$$

Using a linear equation of state of the form $\rho = \rho_0(1 - \beta_T T + \beta_S S)$ (where the variables are dimensional) the circulation (21.46) becomes

$$\Psi = 2\rho_0 T^* \beta_T A \left(-\hat{T} + \frac{\beta_S S^*}{\beta_T T^*} \hat{S} \right). \quad (21.49)$$

Finally, nondimensionalizing time using $\tau = ct$, the equations of motion become

$$\frac{d\hat{T}}{d\tau} = (1 - \hat{T}) - |\Phi|\hat{T}, \quad \frac{d\hat{S}}{d\tau} = \delta(1 - \hat{S}) - |\Phi|\hat{S}, \quad \Phi = -\gamma(\hat{T} - \mu\hat{S}), \quad (21.50a,b,c)$$

where $\Phi = 2\Psi/c$ and the three parameters that determine the behaviour of the system are

$$\gamma = \frac{4\rho_0 T^* \beta_T A}{c}, \quad \delta = \frac{d}{c}, \quad \mu = \frac{\beta_S S^*}{\beta_T T^*}. \quad (21.51)$$

The parameter γ measures the overall strength of the forcing in determining the strength of the circulation, and is the ratio of a relaxation time scale to an advective time scale. The parameter δ is the ratio of the reciprocal time constants of temperature and salinity relaxation, and μ is a measure of the ratio of the effect of the salinity and temperature forcings on the density. Salinity transfer will normally be much slower than heat transfer so that $\delta \ll 1$, whereas if salinity and temperature are both to play a role in the dynamics we need $\mu = \mathcal{O}(1)$. We might also expect both advection and relaxation to be important if $\gamma = \mathcal{O}(1)$, and this will depend on the properties of the capillary tube.

Interpretation

Although the above model describes a potentially real system, one that might be constructed in the laboratory, it is the analogy to aspects of the ocean circulation that interests us here. To make the analogy, we suppose that one box represents the entire high-latitude ocean and the other the entire low-latitude ocean, and the capillary tube and the overflow carry the overturning circulation between them. The reservoirs at $\pm T^*$ and $\pm S^*$ represent the atmosphere. Typically, we would choose the low latitudes to be both heated and salted (the latter because of the low rainfall and high evaporation in the subtropics) and the high latitudes to be cooled and freshened by rainfall. Thus, T^* and S^* have the same sign, and they force the circulation in opposite directions.

It is a common fluid-dynamical experience that the behaviour of a highly-truncated system has little resemblance to that of the corresponding continuous system, and so we expect the model to be only a cartoon of the ocean circulation. For example, we have restricted the circulation to be of basin scale, and the parameterization of the intensity of the overturning circulation by (21.50c) must be regarded with caution, because it represents a frictionally controlled flow rather than a nearly inviscid geostrophic flow. Nevertheless, observations and numerical simulations do indicate that the overturning circulation does have a relatively simple vertical and horizontal structure: the circulation in the North Atlantic is similar to that of a single cell, for example, indicating that an appropriate low-order model may be useful.

One might also question the oceanic appropriateness of the linear relaxation terms. For temperature, the bulk aerodynamic formulae often used to parameterize air-sea fluxes do have a similar form, but the freshening of seawater by rainfall is more akin to an imposed negative flux of salinity, and evaporation is a function of temperature. An alternative might be to impose an effective salt flux so that

$$\frac{d}{dt}(S_1 - S_2) = 2E - 2|\Psi|(S_1 - S_2), \quad (21.52)$$

where E is an imposed, constant, effective rate of salt exchange with the atmosphere. After nondimensionalization, using E/c to nondimensionalize salt, (21.50b) is replaced by

$$\frac{dS}{d\tau} = 1 - |\Phi|S. \quad (21.53)$$

Another aspect of the model that is oceanographically questionable is that the model assumes that the water masses can be mixed below the surface. Thus, when water enters one box from the

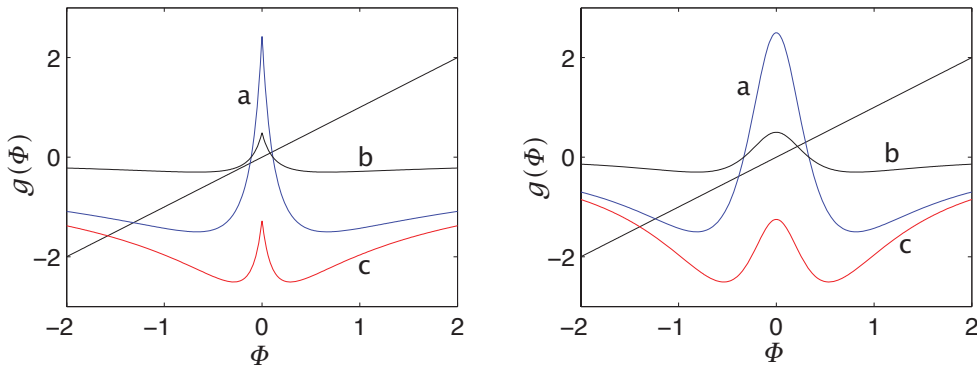


Fig. 21.7 Left panel: graphical solution of the two-box model. The straight line has unit slope and passes through the origin, and is therefore Φ itself. The curved lines plot the function $f(\Phi)$ as given by the right-hand side of (21.54). The intercepts of the two are solutions to the equation. The parameters for the three curves are: a, $\gamma = 5$, $\delta = 1/6$, $\mu = 1.5$; b, $\gamma = 1$, $\delta = 1/6$, $\mu = 1.5$; c, $\gamma = 5$, $\delta = 1/6$, $\mu = 0.75$. Right panel: the same except with Φ^2 in place of $|\Phi|$ on the rhs of (21.54).

other it immediately mixes with its surroundings. Without the stirrer this would not occur and the equations of the box model would not represent a real system. In the real ocean, most of the mixing of water masses happens near the surface (in the mixed layer) and near lateral boundaries or regions of steep topography. Elsewhere in the ocean, mixing is quite small, and probably far from sufficient to mix a large volume of water in the advective or relaxation times of the box model. Having noted all these objections, we will put them aside and continue with an analysis of the model.

Solutions

Equilibria occur when the time-derivatives vanish, and the circulation then satisfies

$$\Phi = g(\Phi) \equiv \gamma \left(\frac{-1}{1 + |\Phi|} + \frac{\mu}{1 + |\Phi|/\delta} \right). \quad (21.54)$$

A graphical solution of this is obtained as the intercept of the right-hand side with the left-hand side, the latter being a straight line through the origin at an angle of 45° , and this is plotted in Fig. 21.7. Perhaps the most interesting aspect of the solutions is that they exhibit *multiple equilibria*; that is, there are multiple steady solutions with the same parameters.

Evidently, for a range of parameters three solutions are possible, whereas for others only one solution exists. Although a fairly complete analysis of the nature of the steady solutions is possible, it is instructive to consider the special case with $\gamma \gg 1$ and $\delta \ll 1$. This corresponds to the situation in which the advective time scale is shorter than the diffusive one and temperature relaxation is much faster than salt relaxation. Using the graphical solution as a guide, two of the solutions are then close to the origin, with $\Phi \ll 1$, and satisfy

$$\Phi \approx \gamma \left(-1 + \frac{\mu\delta}{\delta + |\Phi|} \right), \quad (21.55)$$

giving, for small $|\Phi|$ and $\mu > 1$,

$$\Phi \approx \pm[\delta(\mu - 1)]. \quad (21.56)$$

The positive solution, with flow in the capillary tube from box 1 to box 2, is salinity driven — driven by the density gradient of the same sign as that caused by the salinity, with the density gradient due to temperature opposing the motion. That is, box 1 is denser than box 2 because it

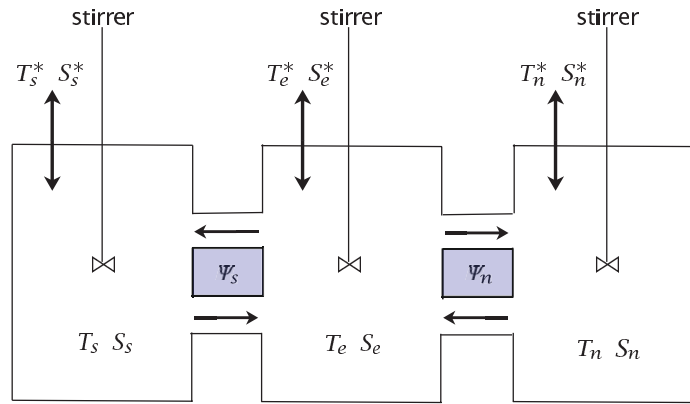


Fig. 21.8 A three-box model. Each box contains fluid with uniform values of temperature and salinity, each exchanges fluid with its neighbour, and in each the temperature and salinity are relaxed toward fixed values.

is more saline, even though it is also warmer. The negative solution is thermally driven, with the flow in the capillary tube going from the denser (cold and fresh) box 2 to the lighter (warm and salty) box 1. However, this solution is unstable, and any small perturbation will amplify and the system will move away from this solution. Solving for temperature and salinity we find that $T \approx 1$ (i.e., it is close to its relaxation value and hardly altered by advection), and $S \approx 1/\mu$.

The third solution has a circulation far from the origin, and the balance in (21.54) is between the left-hand side and the first term on the right. In the limiting case we find

$$\Phi \approx -\sqrt{\gamma}. \quad (21.57)$$

This solution has a density gradient dominated by the temperature effect: the temperature difference is $T \approx 1/\sqrt{\gamma}$ whereas the salinity difference is $S \approx \delta/\sqrt{\gamma}$, and thus its effect on density is much smaller.

21.3.2 ♦ More Boxes

More boxes can be added in a variety of ways and, now forgoing an easy relevance to a laboratory apparatus, one such is illustrated in Fig. 21.8. The three boxes represent the mid- and high-latitude Northern Hemisphere, the mid- and high-latitude Southern Hemisphere, and the equatorial regions. Each of the three boxes can exchange fluid with its neighbour, and each is also in contact with a reservoir and subject to a relaxation to a fixed value of temperature and salinity, (T_s^*, S_s^*) , (T_e^*, S_e^*) and (T_n^*, S_n^*) . Then, with obvious notation, we infer the equations of motion for temperature

$$\begin{aligned} \frac{dT_s}{dt} &= c(T_s^* - T_s) - |\Psi_s|(T_s - T_e), & \frac{dT_n}{dt} &= c(T_n^* - T_n) - |\Psi_n|(T_n - T_e), \\ \frac{dT_e}{dt} &= c(T_e^* - T_e) - |\Psi_s|(T_e - T_s) - |\Psi_n|(T_e - T_n), \end{aligned} \quad (21.58)$$

and similarly for salt, with flow rates given by the density differences

$$\Psi_s = A\rho_0[-\beta_T(T_s - T_e) + \beta_S(S_s - S_e)], \quad \Psi_n = A\rho_0[-\beta_T(T_n - T_e) + \beta_S(S_n - S_e)]. \quad (21.59)$$

These equations may be nondimensionalized and reduced to four prognostic equations for the quantities $T_e - T_n$, $T_e - T_s$, $S_e - S_n$, $S_e - S_s$. Not surprisingly, multiple equilibria can again be found. One interesting aspect is that stable asymmetric solutions arise with symmetric forcing ($T_s^* = T_n^*$, $S_s^* = S_n^*$). These effectively have a pole-to-pole circulation, illustrated in the upper row of Fig. 21.9. Such a circulation can be thought of as the superposition of a thermal circulation in one hemisphere and a salinity-driven circulation in the other.

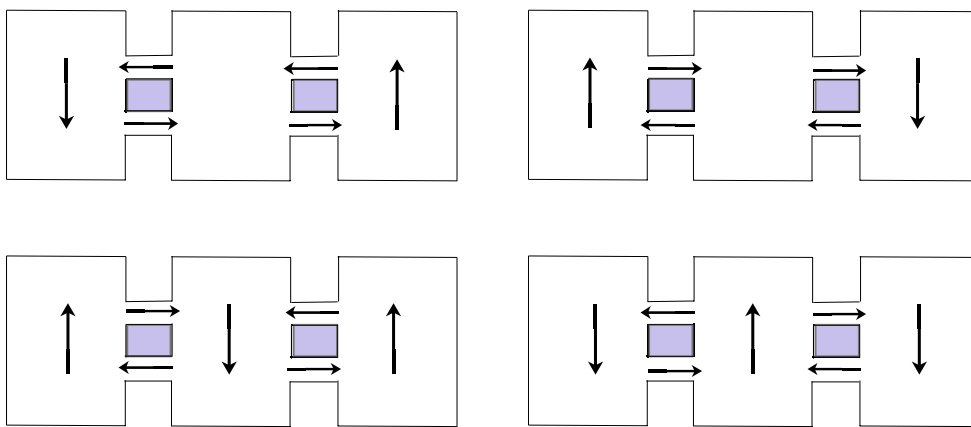


Fig. 21.9 Four solutions to the three-box model with the symmetric forcing $S_s^* = S_n^*$ and $T_n^* = T_s^*$. The two solutions on the top row have an asymmetric, ‘pole-to-pole’ circulation whereas the solutions on the bottom row are symmetric.¹³

The box models are useful because they are suggestive of behaviour that might occur in real fluid systems, and because they provide a means of interpreting behaviour that does occur in more complete numerical models and perhaps in the real world. However, they are by no means good approximations of the real equations of motion and without other supporting evidence the solutions found in box models should not be regarded as representing real solutions of the fluid equations for the world’s oceans.¹⁴ Indeed, the mechanism for the observed pole-to-pole circulation in the real ocean may be quite different from that of the box models — see the sections beginning with sec:windmoc.

21.4 A LABORATORY MODEL OF THE ABYSSAL CIRCULATION

We now return to a more fluid dynamical description of the deep ocean circulation, and consider two simple, closely related, models that are relevant to aspects of the deep circulation, still assuming it to be buoyancy- or mixing-driven. The first, which we consider in this section, is a laboratory model, originally envisioned as being a prototype for the deep circulation. The second model, considered in the following sections, is explicitly a model of the deep circulation. Both models are severe idealizations that describe only limited aspects of the circulation, but they are both very helpful tools that enable us to understand more complete models and, in part, the real circulation itself.

21.4.1 Set-up of the Laboratory Model

Let us consider flow in a rotating tank, as illustrated in Fig. 21.10. The fluid is confined by vertical walls to occupy a sector, and the entire tank rotates anticlockwise when viewed from above, like the Northern Hemisphere. When the fluid is stationary in the rotating frame, the fluid slopes up toward the outer edge of the tank and the balance of forces in the rotating frame is between a centrifugal force pointing outwards and the pressure gradient due to the sloping fluid pointing inwards. In the inertial frame of the laboratory itself, the pressure gradient pointing inwards provides a centripetal force that causes the fluid to accelerate toward the centre of the tank, resulting in a circular motion. (Recall that steady circular motion is always accompanied by an acceleration toward the centre of the circle.)

This set-up, and the accompanying theory, have become known as the *Stommel–Arons–Faller* model.¹⁵ The motivation of the construct is clear, in that the sector represents an ocean basin.

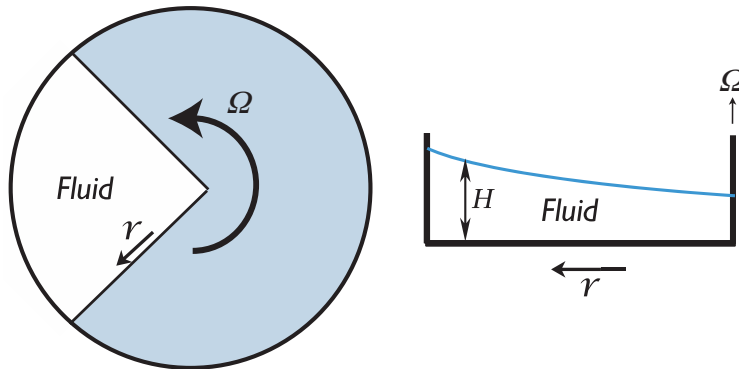


Fig. 21.10 Stommel–Arons–Faller rotating tank experiment. Left: A plan view, with the fluid in the sector at left. Right: Side view. The free surface of the fluid slopes up with increasing radius, giving a balance between the centrifugal force pointing outwards and the pressure force pointing inwards. Small pipes (not shown) provide mass sources and sinks.

However, rather than driving the fluid with wind or by differential heating, we drive it with localized mass sources and sinks, for example from small pipes inserted into the tank. If an oceanic analogy is desired, the mass source might be thought of as representing a source of deep abyssal water due to deep convection. The oceanic analogy is not perfect but it helps build intuition about the real ocean.

21.4.2 Dynamics of Flow in the Tank

Let us assume that the motion of the fluid in the tank is sufficiently weak that its Rossby number is small, and that it obeys the shallow water planetary-geostrophic equations, namely

$$\mathbf{f}_0 \times \mathbf{u} = -g\nabla h + \Omega^2 r \hat{\mathbf{r}} + \mathbf{F}, \quad (21.60a)$$

$$\frac{\partial h}{\partial t} + \nabla \cdot (\mathbf{u}h) = S, \quad (21.60b)$$

where $\mathbf{u} = (v^r, v^\theta)$ is the horizontal velocity in cylindrical (r, θ) coordinates, $\hat{\mathbf{r}}$ is a unit vector in the direction of increasing r , \mathbf{F} represents frictional terms (which we will suppose are small except in boundary layers) and S represents mass sources. These two equations yield the potential vorticity equation,

$$\frac{D}{Dt} \left(\frac{f_0}{h} \right) = \frac{\text{curl}_z \mathbf{F}}{h} - \frac{f_0 S}{h^2}. \quad (21.61)$$

Let us write the height field as

$$h = H(r, t) + \eta(r, \theta, t), \quad (21.62)$$

where $H(r, t)$ is the height field corresponding to the rest state of the fluid (in the rotating frame) and η the perturbation. Thus, from (21.60a)

$$0 = -g\nabla H + \Omega^2 r \hat{\mathbf{r}}, \quad (21.63)$$

which gives

$$H = \frac{\Omega^2 r^2}{2g} + \widehat{H}(t), \quad (21.64)$$

where \widehat{H} is a measure of the overall mass of the fluid. Its rate of change is determined by the mass source

$$\frac{d\widehat{H}}{dt} = \langle S \rangle, \quad (21.65)$$

the angle brackets indicating a domain average. The equations of motion (21.60) become

$$\mathbf{f}_0 \times \mathbf{u} = -g\nabla\eta + \mathbf{F}, \quad (21.66a)$$

$$\frac{\partial}{\partial t}(\eta + H) + \nabla \cdot [\mathbf{u}(\eta + H)] = 0. \quad (21.66b)$$

Equation (21.66a) tells us that, away from frictional regions, the velocity is in geostrophic balance with the pressure field due to the perturbation height η .

Let us now suppose $|\eta| \ll H$ and $|\partial\eta/\partial t| \ll |\partial H/\partial t|$, which holds if the mass source is small and gentle enough. Then (21.66b) may be written

$$\frac{\partial H}{\partial t} + \nabla \cdot (\mathbf{u}H) = 0. \quad (21.67)$$

In this approximation, the potential vorticity equation (21.61) becomes, away from friction and mass sources,

$$\frac{D}{Dt} \left(\frac{f_0}{H} \right) = 0 \quad \text{or} \quad \frac{DH}{Dt} = 0, \quad (21.68a,b)$$

where the second equation follows because f_0 is a constant. (This equation also follows directly from (21.67), because the velocity is geostrophic and divergence-free where friction is absent; however, it is better thought of as a potential vorticity equation, not a mass conservation equation.) Equation (21.68b) means that fluid columns change position in order to keep the same value of H . Further, because H only varies with r , (21.68b) becomes

$$\frac{\partial H}{\partial t} + v^r \frac{\partial H}{\partial r} = 0, \quad (21.69)$$

where the superscript r indicates the radial component of velocity. Using (21.64) and (21.65) then gives

$$v^r = -\frac{g}{\Omega^2 r} \langle S \rangle. \quad (21.70)$$

This is a remarkable result, for it implies that, if $\langle S \rangle$ is positive, the flow is *toward* the apex of the dish, except at the location of the mass sources and in frictional boundary layers, *no matter where the mass source is actually located*. The explanation of this counter-intuitive result is simple enough. If $\langle S \rangle > 0$ the overall height of the fluid increases with time; thus, in order that a given material column of fluid keep its height fixed, it must move toward the apex of the dish. The full velocity may be obtained, away from the frictional regions, using the divergence-free nature of the velocity:

$$\nabla \cdot \mathbf{u} = \frac{1}{r} \left[\frac{\partial(rv^r)}{\partial r} + \frac{\partial v^\theta}{\partial \theta} \right] = 0. \quad (21.71)$$

Then, using (21.70), $\partial v^\theta / \partial \theta = 0$ except at a source or sink, or in a frictional boundary layer. Assuming there is only one frictional boundary layer, $v^\theta = 0$ except at those latitudes (i.e., values of r) that contain a mass source or sink.

To balance the flow toward the apex there must, then, be a *boundary layer* in which the flow has the opposite sense, and therefore in which frictional effects are important. To determine where the boundary layer is — on the east or west side of the domain — we need some vorticity dynamics. Away from the mass source, but including friction, the potential vorticity equation is

$$\frac{D}{Dt} \left(\frac{f_0}{H} \right) = \frac{\text{curl}_z \mathbf{F}}{H} \quad \text{or} \quad -\frac{f_0}{H^2} \frac{DH}{Dt} = \text{curl}_z \mathbf{F}, \quad (21.72a,b)$$

and the free surface of the water slopes downwards toward the apex, as illustrated in Fig. 21.10. Now, suppose that there are a mass source and a sink of equal magnitudes, with the source further from the apex than the sink, as in the panel at the bottom right of Fig. 21.11. The flow from source

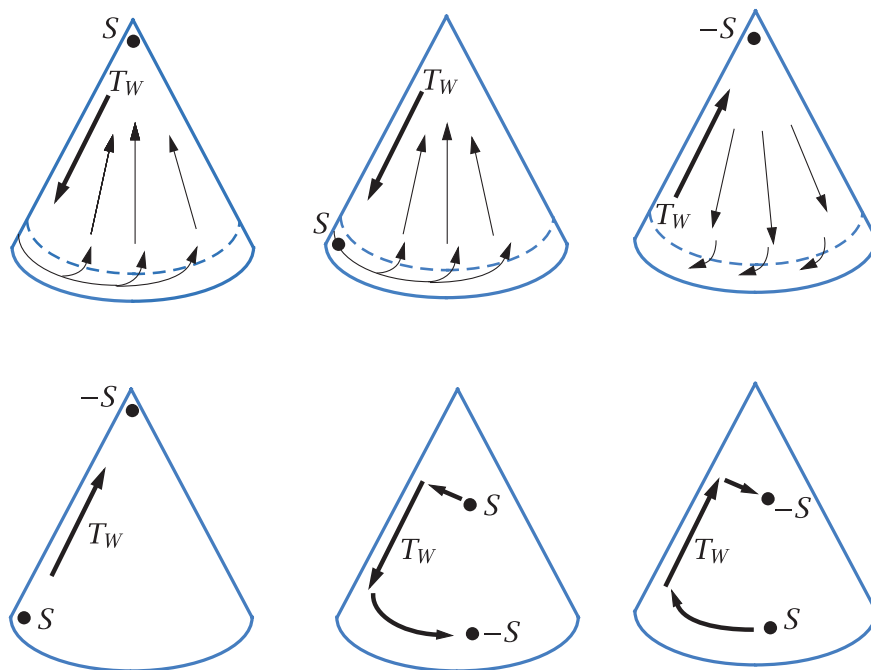


Fig. 21.11 Idealized examples of the flow in the rotating sector experiments, with various locations of a source (S) or sink ($-S$) of mass.

to sink must be along either the left or right boundary of the container. To see which, note that the flow is toward smaller values of H , and therefore the left-hand side of (21.72a) is positive. To balance this, the friction in the boundary current must impart a positive vorticity to the flow (i.e., $\text{curl}_z F > 0$), which means in general that the flow itself must have negative vorticity, and the flow is clockwise. (For example, if $F = -\lambda \mathbf{u}$ the right-hand side of (21.72) is $-(\lambda/H)\text{curl}_z \mathbf{u}$ and this is positive if the flow is clockwise.) Clockwise flow implies a *western* boundary layer, on the left of the container. A western boundary layer is a general feature, not dependent on the placement of mass sources or sinks. For suppose there is a single source of mass, as for example in the upper left example of Fig. 21.11; the interior mass flow will then be toward the apex and the flow in the boundary layer away from the apex. The left-hand side of (21.72a) is then negative, and so $\text{curl}_z F$ must be negative. The flow must then have an anticlockwise sense, again requiring a western boundary layer to achieve a balance in the potential vorticity equation.

The flow is in some ways analogous to flow on the β -plane, and in particular:

- (i) the r -dependence of the height field provides a background potential vorticity gradient, analogous to the β -effect;
- (ii) the time-dependence of H is analogous to a wind curl, since it is this that ultimately drives the fluid motion.

The analogies are drawn out explicitly in the shaded box on page 823; the box also includes a column for abyssal flow in the ocean, discussed in the next two sections.

21.5 A MODEL FOR OCEANIC ABYSSAL FLOW

We will now extend the reasoning applied to the rotating tank to the rotating sphere, and so construct a model — the *Stommel–Arons model* — of the abyssal flow in the ocean.¹⁶ The basic idea is simple: we model the deep ocean as a single layer of homogeneous fluid in which there is a

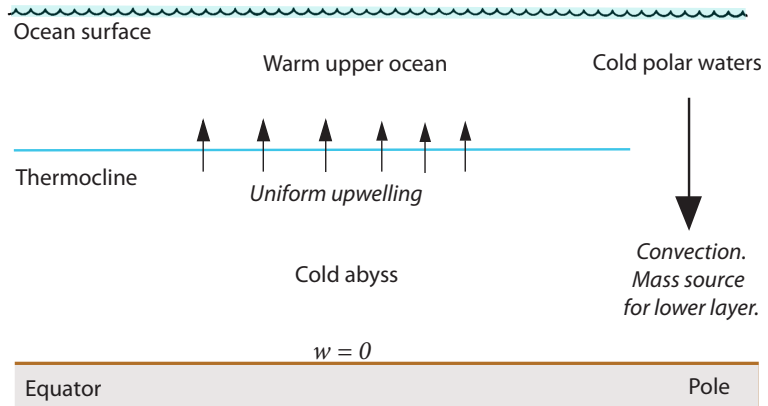


Fig. 21.12 The structure of a Stommel–Arons ocean model of the abyssal circulation. Convection at high latitudes provides a localized mass-source to the lower layer, and upwelling through the thermocline provides a more uniform mass sink.

localized injection of mass at high latitudes, representing convection (Fig. 21.12). However, unlike the rotating dish, mass is extracted from this layer by upwelling into the warmer waters above it, keeping the average thickness of the abyssal layer constant. We assume that this upwelling is nearly uniform, that the ocean is flat-bottomed, and that a passive western boundary current may be invoked to satisfy mass conservation, and which does not affect the interior flow. Obviously, these assumptions are very severe and the model can at best be a conceptual model of the real ocean. Given that, we will work in Cartesian coordinates on the β -plane, and use the planetary-geostrophic approximation.

The momentum and mass continuity equations are

$$\mathbf{f} \times \mathbf{u} = -\nabla_z \phi \quad \text{and} \quad \nabla_z \cdot \mathbf{u} = -\frac{\partial w}{\partial z}, \quad (21.73a,b)$$

where $\mathbf{f} = (f_0 + \beta y)\mathbf{k}$. On elimination of ϕ , (21.73) yields the now-familiar balance,

$$\beta v = f \frac{\partial w}{\partial z}. \quad (21.74)$$

Except in the localized regions of convection, the vertical velocity is, by assumption, positive and uniform at the top of the lower layer, and zero at the bottom. Thus (21.74) becomes

$$v = \frac{f}{\beta} \frac{w_0}{H}, \quad (21.75)$$

where w_0 is the uniform upwelling velocity and H the layer thickness. Thus, the flow is *polewards* everywhere (including the Southern Hemisphere), vanishing at the equator.

21.5.1 Completing the Solution

Since $v = f^{-1}(\partial\phi/\partial x)$, the pressure is given by

$$\phi = \int_{x_0}^x \left(\frac{f^2 w_0}{\beta H} \right) dx', \quad (21.76)$$

where x_0 is a constant of integration, to be determined by the boundary conditions. Because there is no flow into the eastern boundary, x_E , we set $\phi = \text{constant}$ at $x = x_E$, and because this is a one-layer model we are at liberty to set that constant equal to zero. Thus,

$$\phi(x) = - \int_x^{x_E} \left(\frac{f^2 w_0}{\beta H} \right) dx' = -\frac{f^2}{\beta H} w_0 (x_E - x). \quad (21.77)$$

Analogies Between a Rotating Dish, Wind-Driven and Abyssal Flows

Consider homogeneous models of: (i) a rotating dish; (ii) wind-driven flow on the β -plane; and (iii) abyssal flow on the β -plane. We model them all with a single layer of homogeneous fluid satisfying the planetary geostrophic equations. In (i) the mass source, $\langle S \rangle$, is localized and the total depth of the fluid layer changes with time; fluid columns move to keep their depth constant. In (ii) there is no mass source and the depth of the fluid layer is constant; the fluid motion is determined by the wind-stress curl, $\text{curl}_z \boldsymbol{\tau}$, and by β . In (iii) the fluid source (convection) is localized at high latitudes and exactly balanced by a mass loss, S_u , due to upwelling everywhere else, so that layer depth is constant and S_u is uniform and negative nearly everywhere. The equations below then apply away from frictional boundary layers and localized mass sources.

(i) Rotating dish

(ii) Wind-driven flow

(iii) Abyssal flow

PV conservation

$$\frac{D}{Dt} \left(\frac{f_0}{H} \right) = 0 \quad \frac{D}{Dt} \left(\frac{f}{H_0} \right) = \frac{1}{H_0} \text{curl}_z \boldsymbol{\tau} \quad \frac{D}{Dt} \left(\frac{f}{h} \right) = -\frac{fS_u}{h^2}$$

This leads to

$$v^r \frac{\partial H}{\partial r} = -\frac{\partial H}{\partial t} \quad \frac{v}{H_0} \frac{\partial f}{\partial y} = \frac{1}{H_0} \text{curl}_z \boldsymbol{\tau} \quad \frac{v}{h} \frac{\partial f}{\partial y} = -\frac{fS_u}{h^2}$$

and

$$v^r = -\frac{g}{\Omega^2 r} \langle S \rangle \quad v = \frac{1}{\beta} \text{curl}_z \boldsymbol{\tau} \quad v = -\frac{fS_u h}{\beta}$$

$\langle S \rangle$ is localized
mass source

$\text{curl}_z \boldsymbol{\tau}$ is wind stress
curl

S_u is upwelling
mass loss

Meridional mass flow away from boundaries is thus determined by:

sign (and not location) of
localized mass source, $\langle S \rangle$, sign of wind-stress curl,
 $\text{curl}_z \boldsymbol{\tau}$, upwelling and sign of
 f , so polewards if
 $S_u < 0$ (upwelling).

The zonal velocity follows using geostrophic balance,

$$u = \frac{1}{f} \frac{\partial \phi}{\partial y} = \frac{2}{H} w_0 (x_E - x), \quad (21.78)$$

where we have also used $\partial f / \partial y = \beta$ and $\partial \beta / \partial y = 0$. Thus the velocity is eastwards in the interior, and independent of f and latitude, provided x_E is not a function of y .

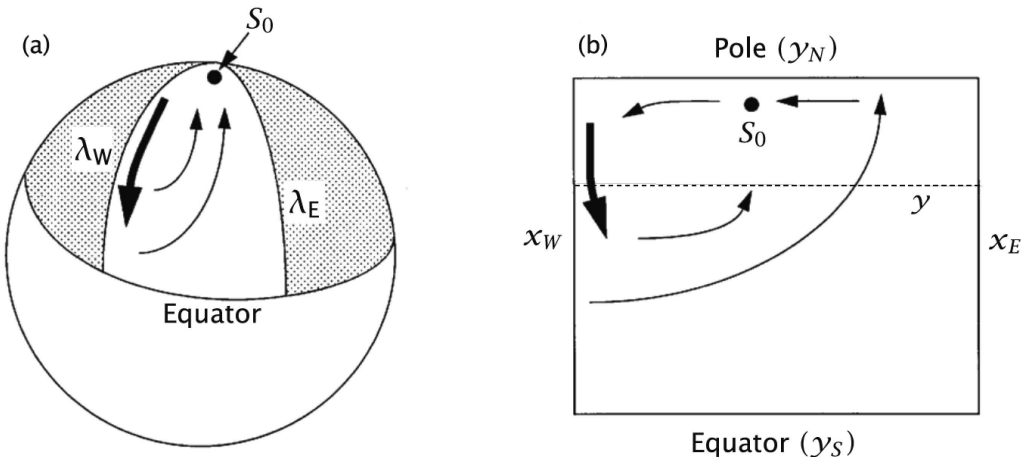


Fig. 21.13 Abyssal circulation in a spherical sector (left) and in a corresponding Cartesian rectangle (right).

Using (21.75) and (21.78) we can confirm mass conservation is indeed satisfied:

$$\frac{\partial u}{\partial x} + \frac{\partial v}{\partial y} + \frac{\partial w}{\partial z} = -\frac{2w_0}{H} + \frac{w_0}{H} + \frac{w_0}{H} = 0. \quad (21.79)$$

21.5.2 Application to the Ocean

Let us consider a rectangular ocean with a mass source at the northern boundary, balanced by uniform upwelling (see Figs. 21.13 and 21.14). Since the interior flow will be northwards, we anticipate a southwards flowing western boundary current to balance mass. Conservation of mass in the area polewards of the latitude y demands that

$$S_0 + T_I(y) = T_W(y) + U(y), \quad (21.80)$$

where S_0 is the strength of the source, T_W the equatorwards transport in the western boundary current, T_I the poleward transport in the interior, and U is the integrated loss due to upwelling polewards of y . Then, using (21.75),

$$T_I = \int_{x_W}^{x_E} vH dx = \int_{x_W}^{x_E} \frac{fw_0}{\beta} dx = \frac{f}{\beta} w(x_E - x_W). \quad (21.81)$$

The upwelling loss is given by

$$U = \int_{x_W}^{x_E} \int_y^{y_N} w dx dy = w_0(x_E - x_W)(y_N - y), \quad (21.82)$$

where y_N denotes the northern (polar) boundary. Assuming the source term is known, then using (21.80) we obtain the strength of the western boundary current,

$$T_W(y) = S_0 + T_I - U = S_0 + \frac{f}{\beta} w(x_E - x_W) - w_0(x_E - x_W)(y_N - y). \quad (21.83)$$

To close the problem we use the fact that over the entire basin mass must be balanced, which gives a relationship between w_0 and S_0 ,

$$S_0 = w_0 \Delta x \Delta y, \quad (21.84)$$

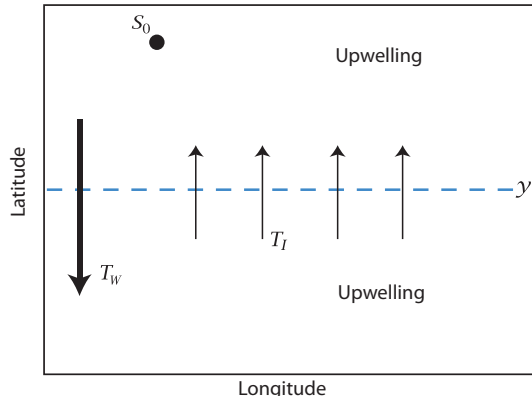


Fig. 21.14 Mass budget in an idealized abyssal ocean. Polewards of some latitude y , the mass source (S_0) plus the poleward mass flux across y (T_I) are equal to the sum of the equatorward mass flux in the western boundary current (T_W) and the integrated loss due to upwelling (U) polewards of y . See (21.80).

where $\Delta x = x_E - x_W$ and $\Delta y = y_N - y_S$, with y_S being the southern boundary of the domain. The strength of the circulation (i.e., the magnitude of S_0 or w_0) is in reality determined by the diffusivity, κ , as previously discussed, and here we take it as a given.

Using (21.84), (21.83) becomes

$$T_W(y) = -w_0 \left(\Delta x(y_N - y) - \frac{f}{\beta} \Delta x - \Delta x \Delta y \right) = w_0 \Delta x \left(y - y_S + \frac{f}{\beta} \right). \quad (21.85)$$

With no loss of generality we will take $y_S = 0$ and $f = f_0 + \beta y$. Then (21.85) becomes

$$T_W(y) = w_0 \Delta x (2y + f_0/\beta), \quad (21.86)$$

or, using $S_0 = w_0 \Delta x y_N$,

$$T_W(y) = \frac{S_0}{y_N} \left(2y - \frac{f_0}{\beta} \right). \quad (21.87)$$

With a slight loss of generality (but consistent with the spirit of the planetary-geostrophic approximation) we take $f_0 = 0$, which is equivalent to supposing that the equatorial boundary of the domain is at the equator, and finally obtain

$$T_W(y) = 2S_0 \frac{y}{y_N}. \quad (21.88)$$

At the northern boundary this becomes

$$T_W(y) = 2S_0, \quad (21.89)$$

which means that the flow southwards from the source is *twice* the strength of the source itself! We also see that:

- (i) the western boundary current is equatorward everywhere;
- (ii) at the northern boundary the equatorward transport in the western boundary current is equal to *twice* the strength of the source;
- (iii) the northward mass flux at the northern boundary is equal to the strength of the source itself.

We may check this last point directly: from (21.81)

$$T_I(y_N) = \frac{\beta y_N}{\beta} w_0 \Delta x = S. \quad (21.90)$$

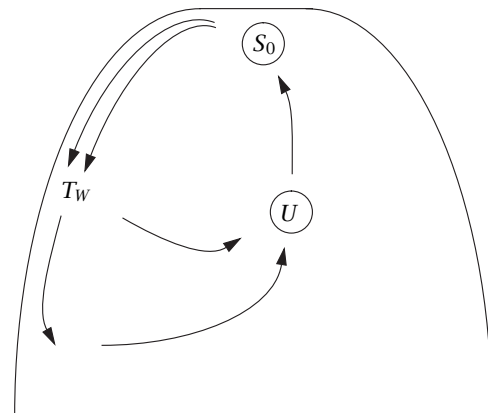


Fig. 21.15 Schematic of a Stommel–Arons circulation in a single sector. The transport of the western boundary current is greater than that provided by the source at the apex, illustrating the property of *recirculation*. The transport in the western boundary current T_W decreases in intensity equatorward, as it loses mass to the polewards interior flow, and thence to upwelling. The integrated sink, due to upwelling, U , exactly matches the strength of the source, S_0 .

The fact that convergence at the pole balances T_W and S_0 does not of course depend on the particular choice we made for f and γ_S .

The flow pattern evidently has the property of *recirculation* (see Fig. 21.15): this is one of the most important properties of the solution, and one that is likely to transcend all the limitations inherent in the model. This single-hemisphere model may be thought of as a crude model for aspects of the abyssal circulation in the North Atlantic, in which convection at high latitudes near Greenland is at least partially associated with the abyssal circulation. In the North Pacific there is, in contrast, little if any deep convection to act as a mass source. Rather, the deep circulation is driven by mass sources in the opposite hemisphere, and we now consider a simple model of this.

21.5.3 A Two-hemisphere Model

Our treatment now is even more obviously heuristic, since our domain crosses the equator yet we continue to use the planetary-geostrophic equations, invalid at the equator. We also persist with Cartesian geometry, even for these global-scale flows. In our defence, we remark that the value of the solutions lies in their qualitative structure, not in their quantitative predictions. Let us consider a situation with a source in the Southern Hemisphere but none in the Northern Hemisphere. For later convenience we take the Southern Hemisphere source to be of strength $2S_0$, and we suppose the two hemispheres have equal area. As before, the upwelling is uniform, so that to satisfy global mass balance S_0 and w_0 are related by

$$S_0 = w_0 \Delta x \Delta y, \quad (21.91)$$

where $\Delta x \Delta y$ is the area of each hemisphere. Then, for a given w_0 , the zonally integrated poleward interior flow in each hemisphere, away from the equator, follows from Sverdrup balance,

$$T_I(y) = \frac{f}{\beta} w_0 (x_E - x_W) = S_0 \frac{y}{y_p}, \quad (21.92)$$

where y_p is either y_N (the northern boundary) or y_S . The western boundary current is assumed to ‘take up the slack’, that is to be able to adjust its strength to satisfy mass conservation. Thus, since $T_I(y_N) = S_0$, where S_0 is half the strength of the source in the *Southern Hemisphere*, it is plain that there must be a southwards flowing western boundary current near the northern end of the Northern Hemisphere, even in the absence of any deep water formation there!

In the northern hemisphere, the total loss due to upwelling polewards of a latitude y is given by

$$U(y) = w_0 \Delta x |y_N - y|. \quad (21.93)$$

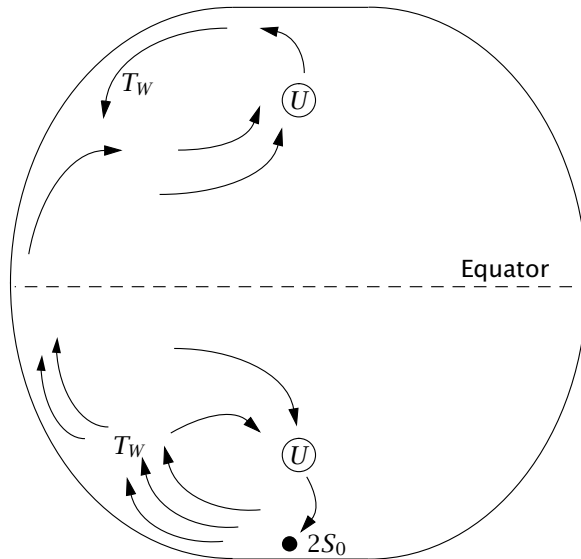


Fig. 21.16 Schematic of a Stommel–Arons circulation in a two-hemisphere basin. There is only one mass source, and this is in the Southern Hemisphere and for convenience it has a strength of 2. Although there is no source in the Northern Hemisphere, there is still a western boundary current and a recirculation. The integrated sinks due to upwelling exactly match the strength of the source.

The strength of the western boundary current is then given by, with southward flow positive,

$$T_W(y) = T_I - U = \frac{f}{\beta} w_0 \Delta x - w_0 \Delta x (y_N - y) = -w_0 \Delta x (y_N - 2y), \quad (21.94)$$

using $f = \beta y$. The boundary current thus changes sign halfway between equator and North Pole, at $y = y_N/2$. [In spherical coordinates, the analogous latitude turns out to be at $\theta = \sin^{-1}(1/2)$.] At the North Pole $y = y_N$ and we have

$$T_W(y_N) = w_0 \Delta x y = S. \quad (21.95)$$

The solution is illustrated schematically in Fig. 21.16. We can (rather fancifully) imagine this to represent the abyssal circulation in the Pacific Ocean, with no source of deep water at high northern latitudes.¹⁷

21.5.4 Summary Remarks on the Stommel–Arons Model

If we were given the location and strength of the sources of deep water in the real ocean, the Stommel–Arons model could give us a global solution for the abyssal circulation. The solution for the Atlantic, for example, resembles a superposition of Fig. 21.15 and Fig. 21.16 (with deep water sources in the Weddell Sea and near Greenland), and that for the Pacific resembles Fig. 21.16 (with a deep water source emanating from the Antarctic Circumpolar Current). Perhaps the greatest success of the model is that it introduces the notions of deep western boundary currents and recirculation — enduring concepts of the deep circulation that remain with us today. For example, the North Atlantic ocean does have a well-defined deep western boundary current running south along the eastern seaboard of Canada and the United States, as seen in Fig. 21.17. However, in other important aspects the model is found to be in error, in particular it is found that there is little upwelling through the main thermocline — much of the water formed by deep convection in the North Atlantic in reality upwells in the Southern Hemisphere.¹⁸ Are there fundamental problems with the model, or just discrepancies in details that might be corrected with a slight reformulation? To help answer that we summarize the assumptions and corresponding predictions of the model, and distinguish the essential aspects from what is merely convenient:

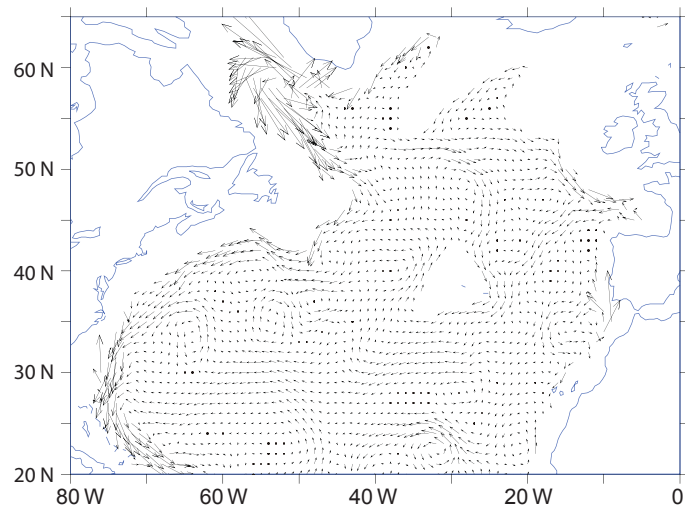


Fig. 21.17 The ocean currents at a depth of 2500 m in the North Atlantic, obtained using a combination of observations and model (as in Fig. 19.3). Note the southwards flowing deep western boundary current.

- (i) A foundational assumption is that of linear geostrophic vorticity balance in the ocean abyss, represented by $\beta v \approx f \partial w / \partial z$, or its shallow water analogue.
 - The effects of mesoscale eddies are thereby neglected. As discussed in Chapter 12, in their mature phase mesoscale eddies seek to barotropize the flow, and so create deep eddying motion that might dominate the deep flow.
- (ii) A second important assumption is that of uniform upwelling, across isopycnals, into the upper ocean, and that $w = 0$ at the ocean bottom. When combined with (i) this gives rise to a poleward interior flow, and by mass conservation a deep western boundary current. The upwelling is a consequence of a finite diffusion, which in turn leads to deep convection as in the model of sideways convection of Section 21.1.
 - The uniform-upwelling assumption might be partially relaxed, while remaining in the Stommel–Arons framework, by supposing (for example) that the upwelling occurs near boundaries, or intermittently, with corresponding detailed changes to the interior flow.
 - If bottom topography is important, then $w \neq 0$ at the ocean bottom. This effect may be most important if mesoscale eddies are present, for then in an attempt to maintain its value of potential vorticity the abyssal flow will have a tendency to meander nearly inviscidly along contours of constant topography. In the presence of a mid-ocean ridge, some of the deep western boundary current might travel meridionally along the eastern edge of the ridge instead of along the coast.
 - The deep water might not upwell across isopycnals, but might move along isopycnals that intersect the surface (or are connected to the surface by convection). If so, then in the presence of mechanical forcing a deep circulation could be maintained even in the absence of a diapycnal diffusivity. The circulation might then be qualitatively different from the Stommel–Arons model, although a linear vorticity balance might still hold, with deep western boundary currents. This is discussed in Section 21.6.

Even if the Stommel–Arons picture were to be essentially correct, we should not consider the deep flow as being driven by deep convection at the source regions. It is a *convenience* to specify the strength of the source term in these regions for the calculations but, just as in the models of sideways convection considered in Section 21.1, the overall strength of the circulation (insofar as it is buoyancy driven) is a function of the size of the diffusivity and the meridional buoyancy gradient at the surface.

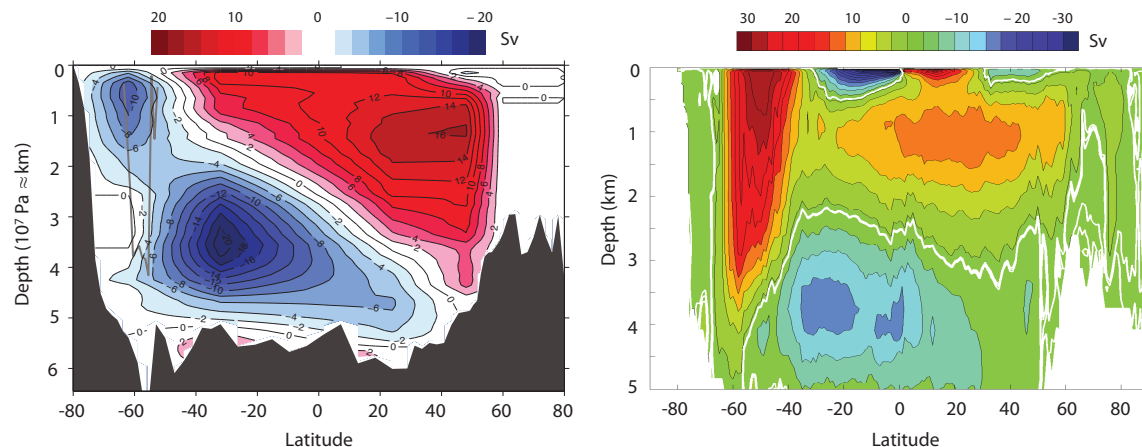


Fig. 21.18 Two independent estimates of the zonally-averaged overturning circulation of the world's ocean. The left panel is from an inverse model that mainly uses hydrographic observations, and shows the residual circulation. The right panel is a state estimation that makes explicit use of a numerical model, and shows the Eulerian circulation.²⁰

21.6† A MODEL OF DEEP WIND-DRIVEN OVERTURNING

There is no need to ask the question 'Is the model true?'. If 'truth' is to be the 'whole truth' the answer must be 'No'. The only question of interest is 'Is the model illuminating and useful?'

George E. Box, *Robustness in the strategy of scientific model building*, 1979.

We previously noted that, with values of the diapycnal diffusivity that are measured in the main thermocline, the theoretical predictions of the MOC are rather weaker than observations suggest. There are two possible resolutions to this problem. One is that the measured diapycnal diffusivity is in fact large in some parts of the ocean (e.g., in the abyss over steep topography), and if this were sufficient to produce the measured overturning and stratification the issue would be resolved. However, such a calculation would likely be fraught with uncertainty. A second and more straightforward resolution would arise if a deep circulation, and deep stratification, could be maintained by a mechanism that was *independent* of the diapycnal diffusivity. This second approach is the one we shall take in for much of the rest of this chapter. Specifically, our goal is to construct and explore models of the overturning circulation of the ocean, and the concomitant deep stratification, that have a 'wind-driven' component that persists even as the diffusivity goes to zero.¹⁹

21.6.1 Observations and Physical Principles

We are motivated by the observation that the MOC is in large part *interhemispheric*, with water sinking at high northern latitudes and upwelling in the Antarctic Circumpolar Current (ACC), as seen for the global circulation in Fig. 21.18 (where the left panel better shows the trajectory of water parcels) and in the Atlantic in Fig. 21.29. The Atlantic MOC (which is the dominant contributor to the global MOC) is dominated by two cells, an upper cell of North Atlantic Deep Water (NADW) with water sinking at about 60° N, moving southwards largely along isopycnals and upwelling in the south. Beneath this cell lies Antarctic Bottom Water (AABW), with sinking at high southern latitudes followed by a deep cross hemispheric circulation and upwelling again in the ACC. We would like to construct a purely wind-driven model that shows these features as simply as possible.

In the absence of a diapycnal diffusivity no upwelling can occur *through* the stratification, because that is a diabatic process. Rather, if there is deep stratification, the deep water must be directly connected to the surface along isopycnals or via a convective pathway, for convection, although

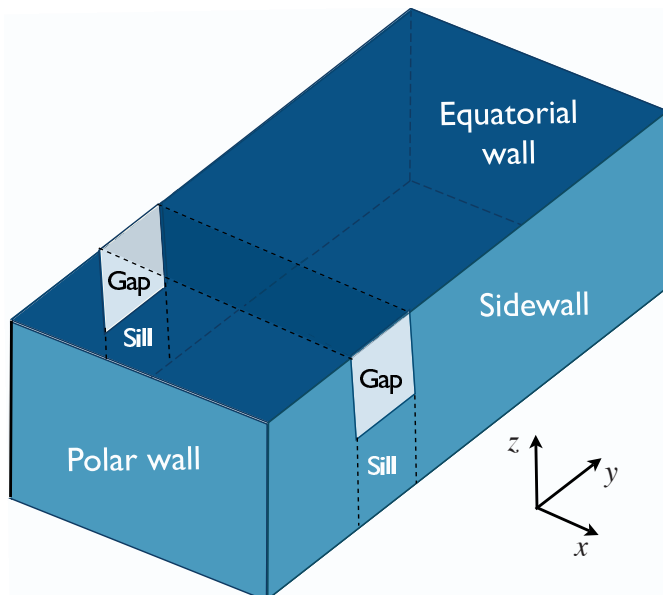


Fig. 21.19 Idealized geometry of the Southern Ocean: a re-entrant channel, partially blocked by a sill, is embedded within a closed rectangular basin; thus, the channel has periodic boundary conditions. The channel is a crude model of the Antarctic Circumpolar Current, with the area over the sill analogous to the Drake Passage.

diabatic, does not rely on a finite eddy diapycnal diffusivity. Let us recall two *de facto* principles about deep circulation:

- (i) A basin will, in the absence of mechanical forcing, tend to fill with the densest available fluid.
- (ii) Light fluid forced down by wind may displace the cold fluid, so producing stratification.

A completely closed ocean thus fills completely with dense polar water, except in the upper several hundred metres where the main thermocline forms. However, suppose that the polewards part of the basin is not fully enclosed but is periodic, as illustrated in Fig. 21.19, with a sill across it at mid-depth, and suppose too that the surface temperature decreases monotonically polewards. A fully enclosed basin exists only beneath the level of the sill, and we may expect the densest water in the basin, formed at the polewards edge of the domain, to fill the basin only below the level of the sill, and that above this may lie warmer water with origins at lower latitudes. Furthermore, suppose that an eastward wind blows over the channel that produces an equatorial flow in the Ekman layer. Then mass conservation demands that there must exist a *subsurface* return flow, and thus a meridional overturning circulation is set up. Note the essential role of the channel in this: if the gap were closed, then the return flow could take place at the surface via a western boundary current, as in a conventional subpolar gyre, and no overturning circulation need be set up. But in a zonally-periodic channel, an eastward wind produces a northward Ekman flow that can only be balanced by a return flow at depth — that is, a meridional overturning circulation.

21.6.2 A Single-hemisphere Model

Let us first a single-hemisphere basin with a periodic channel near its poleward edge. We suppose the basin to be in the southern hemisphere, so the channel represents the Antarctic Circumpolar Current (ACC), and that the dynamics are Boussinesq and planetary-geostrophic. We will choose extremely simple forms of wind and buoyancy forcing to allow us to obtain an analytic solution, and then later discuss how the qualitative forms of these solutions might more apply generally.

Wind and buoyancy forcing

Thermodynamic forcing is imposed by fixing the surface buoyancy, b_s . (In the discussion following salinity is absent, and buoyancy is virtually equivalent to temperature.) South of the gap we

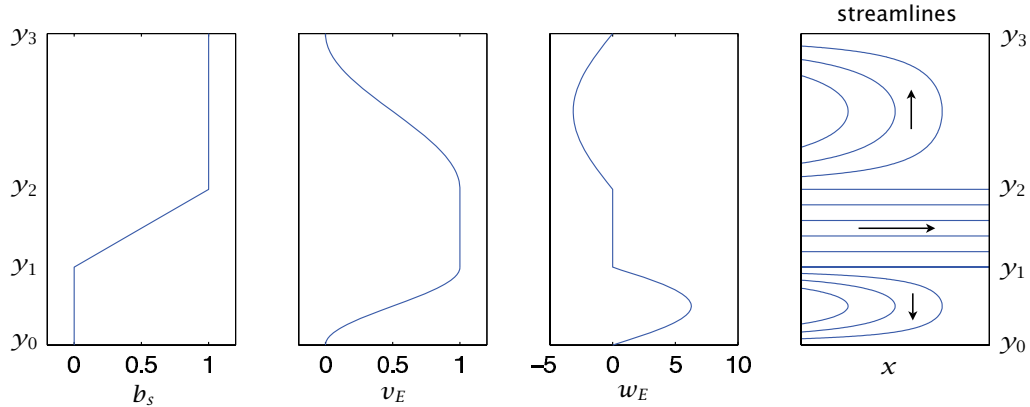


Fig. 21.20 The surface buoyancy b_s , meridional Ekman velocity v_E , vertical Ekman velocity w_E and the solution streamlines for the geostrophic horizontal flow, omitting the western boundary currents. The ordinate in all plots is latitude, with the pole at the bottom, and the four fields are given by, respectively, (21.96), (21.97a), (21.97b) and (21.98), with purely zonal flow given by (21.101) in the channel.

suppose the buoyancy to be constant, then that it increases linearly across the gap, and is constant again polewards of the gap. Thus, there is no temperature gradient across the subtropical gyre, focusing attention on the influence of the channel. Thus, referring to Fig. 21.20 or Fig. 21.21 for the definitions of the geometric factors,

$$b_s = \begin{cases} b_1, & y_0 \leq y \leq y_1, \\ b_1 + \frac{(b_2 - b_1)(y - y_1)}{y_2 - y_1}, & y_1 \leq y \leq y_2, \\ b_2, & y \geq y_2, \end{cases} \quad (21.96)$$

where $b_2 > b_1$, and both are constants, and we may take $b_1 = 0$ and $y_0 = 0$.

The wind forcing is purely zonal, and it is convenient to express this in terms of the Ekman transport and associated pumping (refer to section 5.7). In the channel the Ekman transport is chosen to be (realistically) equatorward and (less realistically) constant, a simplification that avoids complications of wind-driven upwelling in the channel. South (polewards) of the channel there is a conventional subpolar gyre, with an Ekman upwelling and an equatorward Ekman transport that joins smoothly to that of the channel. Equatorwards of the channel there is a conventional subtropical gyre, with Ekman downwelling. All this may be achieved by specifying:

$$v_E = \begin{cases} \frac{V}{2} \left[1 - \cos \left(\frac{\pi y}{\Delta y_1} \right) \right] & 0 \leq y < y_1 \\ V & y_1 \leq y < y_2 \\ \frac{V}{2} \left[1 + \cos \left(\frac{\pi(y - y_2)}{\Delta y_2} \right) \right] & y_2 \leq y < y_3 \end{cases} \quad w_E = \begin{cases} W_1 \sin \left(\frac{\pi y}{\Delta y_1} \right) & 0 \leq y < y_1 \\ 0 & y_1 \leq y < y_2 \\ -W_2 \sin \left(\frac{\pi(y - y_2)}{\Delta y_2} \right) & y_2 \leq y < y_3, \end{cases} \quad (21.97a,b)$$

where $\Delta y_1 = y_1$, $\Delta y_2 = y_3 - y_2$, and V is a constant that determines the magnitude of the meridional Ekman flow. The meridional Ekman transport, v_E , is related to the Ekman pumping by $w_E/\delta_E = \partial v_E/\partial y$, so that $W_i = \delta_E \pi V / (2\Delta y_i)$, where δ_E is the Ekman layer thickness. If f were constant, the wind-stress curl would be proportional to the w_E field above. The precise details of the forcing do not affect the qualitative form of the solution — they merely allow an analytic solution to be obtained — but there are two essential aspects to it:

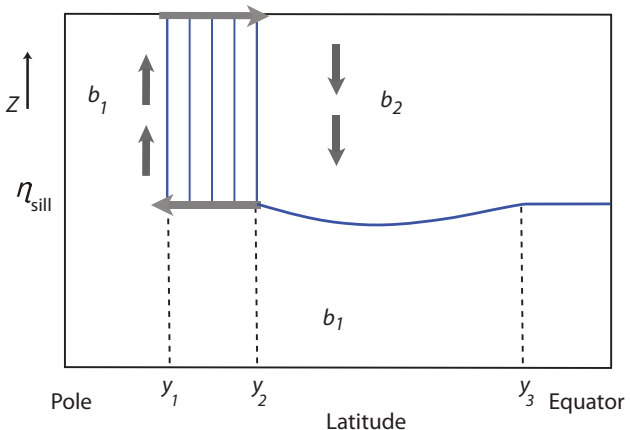


Fig. 21.21 Cross-section of the structure of the single-hemisphere ocean model described in Section 21.6.2. The domain is zonally closed equatorwards of y_2 and polewards of y_1 , with a zonally periodic channel between latitudes y_1 and y_2 and above the sill, which has height η_{sill} . The arrows indicate the fluid flow driven by the equatorward Ekman transport in the channel, and the solid lines are isopycnals.

- (i) The surface is cold south of the channel, warm north of the channel, and there is a temperature gradient across the channel.
- (ii) The Ekman flow is equatorwards within the channel, with conventional gyres to either side. The meridional extent of the region south of the channel and the wind forcing within it are relatively unimportant, and the region could be shrunk to nearly zero.

Solution in the gyres

Below the depth of the sill the basin is fully enclosed, and therefore up to that level the basin will fill with the densest available water (much as described in Section 21.1), except where it may be displaced by warmer fluid equatorward of the gap that is pumped down below the level of the sill by the wind (Fig. 21.21). Thus, all of the domain south of the channel, and nearly everywhere below the sill, the water has buoyancy b_1 . Polewards of the channel, then, the fluid is barotropic and its vertically integrated horizontal circulation is given by Sverdrup balance, $\beta V = f w_E / H$, where V is the vertically integrated flow. With the wind stress of (21.97) we get a conventional barotropic subpolar gyre (and associated western boundary current) by the same methods that we employed in Chapter 19.

Above the sill, net meridional geostrophic transfer is forbidden in the channel region, because by geostrophic balance $f \bar{v}_g = \partial \bar{\phi} / \partial x = 0$, where ϕ is the pressure and the overbar denotes a zonal average. Equatorward of the channel the region above the sill will therefore tend to fill with the densest water available to it, and this is water with buoyancy equal to b_2 (which is the buoyancy of the water as it emerges from the channel). However, because of the presence of wind forcing, the base of this layer is not flat; rather, this fluid obeys the dynamics of the reduced-gravity single-layer ventilated thermocline model discussed in Section 20.7.1. In such a model the depth of the fluid on the eastern boundary is constant, and this must be specified. Here, this is given by the height of the sill, and therefore $h(x = x_e, y) = h_e = H - \eta_{\text{sill}}$, where H is the total depth of the basin and η_{sill} is the sill height. Then, using (20.92) and (21.97), the thickness of the moving layer equatorward of the sill is given by, for $y_2 < y < y_3$,

$$h^2 = D^2(x, y) + h_e^2, \quad (21.98)$$

where

$$D^2 = -\frac{2f^2}{g' \beta} \int_x^{x_e} w_E \, dx' = \frac{2f^2}{g' \beta} W_2(x_e - x) \sin\left(\frac{\pi(y - y_2)}{\Delta y_2}\right), \quad (21.99)$$

with $g' = b_2 - b_1$. The solution is closed by the addition of a western boundary current. Note that because $h > h_e$, the light fluid is pushed below the level of the sill in the subtropical gyre.

Solution in the channel

In the channel, the fluid in the Ekman layer flows equatorward, and therefore there must be a compensating poleward flow at depth. This will occur just below the level of the sill: it cannot be deeper, because here the basin is full of denser, b_1 fluid, and in the absence of eddying or ageostrophic flow it cannot be shallower because of the geostrophic constraint. Now, because of the temperature gradient across the channel the polewards flowing fluid is warmer than the fluid at the surface, and therefore convectively unstable. Convection ensues, the result of which is the entire column of fluid between the top of the sill and the surface mixes and takes on the temperature of the surface. Thermal wind demands that there be a zonal flow associated with this meridional temperature gradient, so this temperature distribution is advected eastwards into the interior of the channel. Because the interior is presumed to be adiabatic, this temperature field extends zonally throughout the channel. Thus, in steady state, the temperature *everywhere* in the channel above the level of the sill is given by

$$b(x, y, z) = b_s(y) = b_1 + \frac{(b_2 - b_1)(y - y_1)}{y_2 - y_1}, \quad y_1 \leq y \leq y_2, \quad z > \eta_{sill}. \quad (21.100)$$

Convective mixing does not rely on a diapycnal diffusivity other than a molecular one: convective plumes are generally turbulent, generating small scales in the fluid interior where mixing and entrainment may occur; failing that, the lighter fluid is displaced to the surface where it cools by way of interaction with the atmosphere. The zonal velocity within the channel is then given by thermal wind balance, so that

$$u(x, y, z) = -\frac{1}{f} \left(\frac{b_2 - b_1}{y_2 - y_1} \right) (z - \eta_{sill}), \quad (21.101)$$

and since $f < 0$ the shear, $\partial u / \partial z$, is positive.

Regarding the depth-integrated zonal momentum budget, the wind stress at the surface is balanced by a pressure force against the sill walls. This pressure gradient arises through the meridional circulation, as the southward return flow just below the level of the sill is associated with a zonal pressure gradient that is exactly equal, but opposite, to the stress exerted by the wind. That is to say, in the Ekman layer the wind stress is balanced by the Coriolis force on the equatorward flow in the Ekman layer, which by mass conservation is equal and opposite to the Coriolis force on the deep poleward flow, which by geostrophy is equal to the net pressure force on the sill walls. The wind stress plays no role in determining the zonal transport of the channel: if the wind increases, the meridional overturning and the pressure force increase but with no change to the transport. This is a somewhat unrealistic feature of the model, for in reality the form stress induced by the flow over bottom topography (and that balances the wind stress) is likely to be a function of the zonal transport as well as the meridional transport.

A qualitative summary

The circulation of the model may be described as follows. The entire basin polewards of the channel fills with dense, b_1 , water. Below the sill this fluid extends equatorward, filling the lower part of the channel and subtropical basin, up to the level of the sill. Now, Ekman pumping in the channel forces near-surface fluid equatorward, which warms as it goes, entering the subtropical basin with buoyancy b_2 . This fluid fills the basin down to the level of the sill, where it encounters the dense, b_1 , fluid. The subtropical basin is wind-driven, and it forms a subtropical gyre with a single moving layer. Its dynamics are completely determined by specifying the wind, the reduced gravity ($g' = b_2 - b_1$), and the depth of the fluid at the eastern boundary (the sill depth). Because of the requirements of mass conservation, there must be a poleward return flow at depth, and so at the level of the sill warm water flows polewards. This flow is convectively unstable (because the water is lighter than that at the surface), and so the entire column of fluid mixes and its density takes on the value at the surface. The meridional temperature gradient gives rise to an eastward flow,

and this temperature field is advected zonally, and in steady state the temperature distribution is zonally symmetric and given by (21.100). The overturning circulation within the ACC is known as the Deacon Cell, and this is a crude model of it. It is considered further in Section 21.7.

If the diapycnal diffusivity were non-zero, the sharp boundary between the two fluid masses at the sill height would be diffused to a front of finite thickness, with some upwelling and water mass transformation occurring across the front. This diffusive loss of dense fluid would be compensated by water-mass formation at the surface, polewards of the channel, leading to a deep, diffusively-driven circulation. That is, the deep water mass of b_1 fluid would circulate: this is a crude model of the ‘Antarctic Bottom Water’ cell.

Suppose now that the wind were everywhere zero, and the diffusivity small but non-zero. The cold, b_1 fluid would quickly completely fill the basin polewards of the channel, and would also fill the basin equatorward of the channel up to the level of the sill. However, with no wind to drive an overturning circulation dense b_1 water would slowly drift ageostrophically across the channel, displacing any warmer water until the *entire basin* were filled with the dense, b_1 , fluid, except for a thin boundary layer at the top needed to satisfy the upper boundary condition. The final state would be one of no motion, and no stratification, below this boundary layer.

The important overall conclusion to be drawn is the following: *a deep meridional circulation and a deep stratification can be maintained, even as the diapycnal diffusivity goes to zero, in the presence of a wind forcing and a circumpolar channel.* Of course there are a number of idealized or unrealistic aspects to this model, perhaps the most egregious being:

- The vertical isopycnals in the channel will be highly baroclinically unstable. This will cause the isopycnals to slump and will potentially set up an eddy-induced circulation. We consider this at length later on.
- This model has no surface temperature gradient across the subtropical gyre. If one were present, it would lead to the formation of a ‘main’ subtropical thermocline, a full treatment of which would require determining its eastern boundary conditions. This would not qualitatively affect the presence of a deep, wind-driven overturning circulation.
- The wind stress in the model channel is chosen so that the meridional Ekman transport is constant. (This means the wind stress is chosen to vary in the same fashion as the Coriolis parameter, and if f were constant, the wind-stress curl would vanish.) Thus, there is no wind-driven downwelling or upwelling in the channel, and this simplifies the solution. Numerical simulations suggest that this choice does not affect the qualitative nature of the overturning circulation or temperature distribution.

21.6.3 A Cross-equatorial Wind-driven Deep Circulation

We qualitatively and heuristically extend the above model to consider flow across the equator. Thus, we suppose that the ocean basin extends to high northern latitudes, where there is, potentially, another source of cold deep water. To keep the model simple and tractable we will assume a very simple buoyancy structure:

$$b_s = \begin{cases} b_1, & 0 \leq y \leq y_1, \\ b_1 + \frac{(b_2 - b_1)(y - y_1)}{y_2 - y_1}, & y_1 \leq y \leq y_2, \\ b_2, & y_2 \leq y \leq y_4, \\ b_3 & y > y_4, \end{cases} \quad (21.102)$$

where the geometry is illustrated in Fig. 21.22. Given that $b_2 > b_1$, there are three cases to consider:

- (i) $b_3 > b_2$. This is not oceanographically relevant to today’s climate, nor does it provide another potential deep water source.

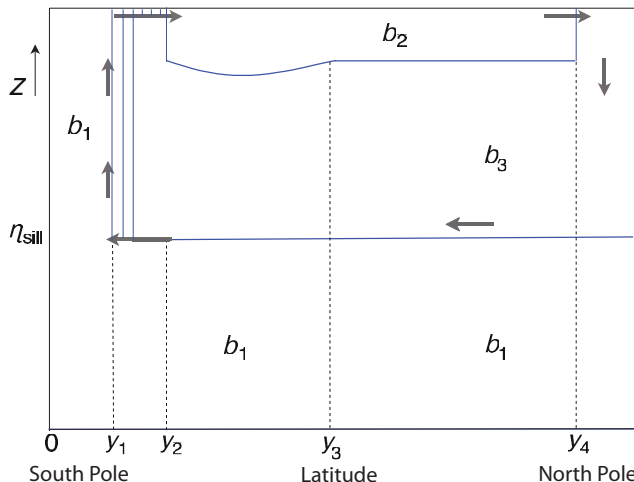


Fig. 21.22 As for Fig. 21.21, but now for a two-hemisphere ocean with a source of dense water, b_3 , at high northern latitudes. The solid lines are isopycnals, and here the wind is zero in the Northern Hemisphere.

- (ii) $b_3 < b_1$. The northern water is now the densest in the ocean, and would fill up the entire basin north of the channel (except near the surface in regions where some b_2 water is pushed down by the wind), and so provide no mid-depth stratification.
- (iii) $b_1 < b_3 < b_2$. This is the most interesting and relevant case, and the only one we explore further.

As regards the wind, we will assume that south of the equator this is given by (21.97). North of the equator the wind forcing does not affect the qualitative nature of the overturning circulation, and may be taken to be zero.

Descriptive solution

In case (iii), the entire basin below the sill fills with b_1 water, except where wind forcing forces warmer fluid below the sill level, as before. However, unlike the earlier case, the fluid above the sill is predominantly b_3 water from high northern latitudes. This forms in high polar latitudes and fills most of the basin above the sill, from the basin boundary in the north to the channel in the south (as discussed more below). However, except at latitudes where the b_3 is formed, it does not reach the surface because of the presence of b_2 water. That water is pushed down by the wind in the southern hemisphere to some as yet undetermined depth (discussed below), the boundary between b_2 and b_3 water then forming the upper ocean thermocline.

These water masses circulate because of the wind forcing in the channel. As in the single-hemisphere case, northwards flowing water emerges from the channel with buoyancy b_2 . This emerges into a region of Ekman downwelling, with a northward transport carried by a western boundary current. This transport crosses the equator finally reaching the latitudes where b_3 water is formed where it sinks and returns equatorward, again in a western boundary current. (Away from the western boundary layer there is no meridional flow in the absence of diffusion, because the flow satisfies $\beta v = f \partial w / \partial z$ and there is no upwelling.) This water then crosses the sill. However, unlike the single-hemisphere case, in the northern part of the sill this water is denser than the surface water; no convection occurs and so the b_3 water extends upwards to the surface, where it warms by contact with the atmosphere and is advected equatorward to become b_2 water. Further south the surface buoyancy in the channel is less than b_3 , and the column now mixes convectively, much as in the single-hemisphere case. The solution is completed by specifying the thickness of the layer of b_2 water at the surface. Now, if the circulation is in steady state, the meridional transport between the gyres must equal that of the northward Ekman flow at the northern edge of the circumpolar channel, and given the wind forcing, this is determined by the depth of the layer at the eastern

boundary, a constant. Thus, in this model, global constraints determine the depth of the eastern boundary of the thermocline.

Suppose that the wind were everywhere zero. Then, as in the single-hemisphere case, the circulation would eventually die. Again, though, slow ageostrophic motion across the channel would first allow the entire basin, within and on both sides of the channel, to fill with the densest available water, and in the final steady state there would be no stratification (and no motion) below a thin surface layer.

Suppose, on the other hand, that a small amount of diffusion were added to the wind-forced model above. Then there would be mass exchange between the layers and, in particular, the deep cell of b_1 water would begin to circulate diffusively. In addition, the mid-depth cell would begin to upwell through the b_2 – b_3 interface, and develop a diffusively driven circulation, in much the same way as is illustrated in Fig. 20.15.

Summary remarks

The key result of this model is that, even as the diffusivity falls and the interior of the ocean becomes more and more adiabatic, a meridional cross-hemispheric circulation can be maintained, provided that the wind across the circumpolar channel remains finite. The diabatic water mass transformations all occur at the surface or in convection: these processes require a non-zero diffusivity, but this can be the molecular diffusivity because the associated mixing involves turbulence, which can generate arbitrarily small scales. (Note also that the convection that occurs in the circumpolar channel reduces the potential energy of the column, and requires no mechanical input of energy.) Aside from the region of the ACC, the meridional transport will occur (in this model) in western boundary layers. Indeed, we may still expect to see a southwards flowing deep western boundary current south of y_4 and below the b_2 water in Fig. 21.22, just as in the implicitly diffusive Stommel–Arons model. In the ACC itself, the meridional transport occurs in a subsurface current, nestled against the sill. Although the overturning circulation in this model is ‘wind-driven’, the possibility that it may be cross-equatorial depends upon the thermodynamic forcing; in particular, if there is no source of dense water in the northern hemisphere, then the basin above the sill simply fills with b_2 water, as in the model of Section 21.6.2, and there need be little or no interhemispheric flow. We emphasize, too, that our model of interhemispheric flow is quite heuristic: we have essentially *posited* that b_2 water may continuously flow across the equator, possibly in a western boundary current but without examining the equatorial dynamics at all.

The ACC plays a key role in the above description but we have grossly oversimplified it. In particular, the nearly vertical isopycnals of the model will be highly baroclinically unstable, and this provides a convenient segue into our next topic.

21.7 THE ANTARCTIC CIRCUMPOLAR CURRENT

We now take a closer look at the Antarctic Circumpolar Current (ACC) itself, with a focus on its own internal dynamics; we come back to the connection with the rest of the world’s oceans in Section 21.8. The ACC system, sketched in Fig. 21.23, differs from other oceanic regimes primarily in that the flow is, like that of the atmosphere, predominantly zonal and re-entrant. The two obvious influences on the circulation are the strong, eastward winds (the ‘roaring forties’ and the ‘furious fifties’) and the buoyancy forcing associated with the meridional gradient of atmospheric temperature and radiative effects that cause ocean cooling at high latitudes and warming at low ones. Providing a detailed description of the resulting flow is properly the province of numerical models, and here our goals are much more modest, namely to describe and understand some of the fundamental dynamical mechanisms that determine the structure and transport of the system, with a view to then connecting the ACC to the rest of the world’s oceans.²²

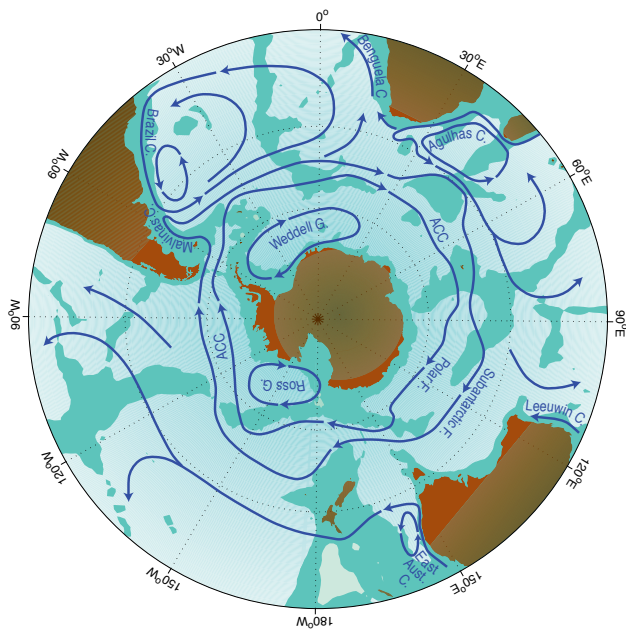


Fig. 21.23 The major currents in the Southern Ocean. Notable are the South Atlantic subtropic gyre and the two main cores of the ACC, associated with the Polar front and the sub-Antarctic front.²¹

21.7.1 Steady and Eddying Flow

Consider again the simplified geometry of the Southern Ocean as sketched in Fig. 21.19. The ocean floor is flat, except for a ridge (or ‘sill’) at the same longitude as the gyre walls; this is a crude representation of the topography across the Drake Passage, that part of the ACC between the tip of South America and the Antarctic Peninsula. In the planetary-geostrophic approximation, the steady response is that of nearly vertical isopycnals in the area above the sill, as illustrated in Fig. 21.21. Below the sill a meridional flow can be supported and the isotherms spread polewards, as illustrated in the left panel of numerical solutions using the primitive equations (Fig. 21.24).²³

The stratification of the non-eddying simulation is similar to that predicted by the idealized model illustrated in Fig. 21.21. However, the steep isotherms within the channel contain a huge amount of available potential energy (APE), and the flow is highly baroclinically unstable. If baroclinic eddies are allowed to form, the solution is dramatically different: the isotherms slump, releasing that APE and generating mesoscale eddies that exercise control over much of the circulation. An important conclusion is that *baroclinic eddies are of leading-order importance in the dynamics of the ACC*. A dynamical description of the ACC without eddies would be *qualitatively* in error, in much the same way as would a similar description of the mid-latitude troposphere (i.e., the Ferrel Cell). These eddies transfer both heat and momentum, and much of the rest of our description will focus on their effects.

21.7.2 Vertically Integrated Momentum Balance

The momentum supplied by the strong eastward winds must somehow be removed. Presuming that lateral transfers of momentum are small the momentum must be removed by fluid contact with the solid Earth at the bottom of the channel. Thus, let us first consider the vertically integrated momentum balance in a channel, without regard to how the momentum might be vertically transferred. We begin with the frictional-geostrophic balance, namely

$$\mathbf{f} \times \mathbf{u} = -\nabla\phi + \frac{\partial \tilde{\tau}}{\partial z}, \quad (21.103)$$

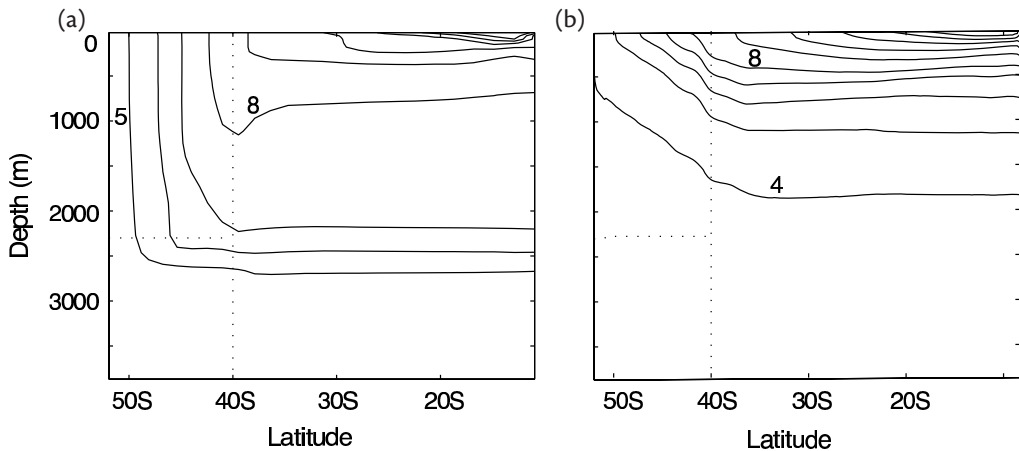


Fig. 21.24 The zonally averaged temperature field in numerical solutions of the primitive equations in a domain similar to that of Fig. 21.19 (except that here the channel and sill are nestled against the poleward boundary). Panel (a) shows the steady solution of a diffusive model with no baroclinic eddies, and (b) shows the time averaged solution in a higher-resolution model that allows baroclinic eddies to develop. Two contour values in each panel are labelled. The dotted lines show the channel boundaries and the sill.²⁴

where $\tilde{\tau}$ is the kinematic stress, τ/ρ_0 , and $\phi = p/\rho_0$. Integrating over the depth of the ocean and using Leibniz's rule (that is, $\nabla \int_{\eta_B}^0 \phi dz = \int_{\eta_B}^0 \nabla \phi dz - \phi_B \nabla \eta_B$), gives

$$\mathbf{f} \times \hat{\mathbf{u}} = -\nabla \hat{\phi} - \phi_b \nabla \eta_b + \tilde{\tau}_w - \tilde{\tau}_f, \quad (21.104)$$

where $\tilde{\tau}_w$ is the stress at the surface (due mainly to the wind) and $\tilde{\tau}_f$ is the frictional stress at the bottom, a hat denotes a vertical integral and ϕ_b is the pressure at $z = \eta_b$, where η_b is the z -coordinate of the bottom topography. The x -component of (21.104) is

$$-f \hat{v} = -\frac{\partial \hat{\phi}}{\partial x} - \phi_b \frac{\partial \eta_b}{\partial x} + \tilde{\tau}_w^x - \tilde{\tau}_f^x, \quad (21.105)$$

and on integrating around a line of latitude the term on the left-hand side vanishes by mass conservation and we are left with

$$-\overline{\phi_b \frac{\partial \eta_b}{\partial x}} + \overline{\tilde{\tau}_w^x} - \overline{\tilde{\tau}_f^x} = 0, \quad (21.106)$$

where overbars denote zonal averages. The first term is the bottom, or topographic, form drag, encountered in Sections 3.6 and 19.6, and observations and numerical simulations indicate that it is this, rather than the frictional term $\tilde{\tau}_f^x$, that predominantly balances the wind stress.²⁵ We address the question of *why* this should be so in section 21.7.5.

The vorticity balance is similarly dominated by a balance between bottom form-stress curl and wind-stress curl. Taking the curl of (21.104), noting that $\nabla \cdot \hat{\mathbf{u}} = 0$, gives

$$\beta \hat{v} = -\mathbf{k} \cdot \nabla \phi_b \times \nabla \eta_b + \text{curl}_z \tilde{\tau}_w - \text{curl}_z \tilde{\tau}_f. \quad (21.107)$$

Now, on integrating over an area bounded by two latitude circles and applying Stokes' theorem the β -term vanishes by mass conservation and we regain (21.106). This means that *Sverdrup balance, in the usual sense of $\beta v \approx \text{curl}_z \tilde{\tau}_w$, cannot hold in the zonal average*: the left-hand side vanishes but the right-hand side does not. The same could be said for the zonal integral of (21.107) across a

gyre, but the two cases do differ: In a gyre Sverdrup balance can (in principle) hold over most of the interior, with mass balance being satisfied by the presence of an intense western boundary current. In contrast, in a channel where the dynamics are zonally homogeneous then v must be, on average, zero at *all* longitudes and form drag and/or frictional terms must balance the wind-stress curl in a given water column. Sverdrup balance is thus a less useful foundation for channel dynamics — at least zonally homogeneous ones — than it is for gyres. Of course, the real ACC is *not* zonally homogeneous, and may contain regions of poleward Sverdrup flow balanced by equatorward flow in boundary currents along the eastern edges of sills and continents, and the extent to which Sverdrup flow is a leading-order descriptor of its dynamics is a matter of geography (and debate!). See also Section 21.7.6.

Even though topographic drag may be dominant in removing momentum, non-conservative frictional terms cannot be neglected, for two reasons. First, they are the means whereby kinetic energy is dissipated. Second, if there is a contour of constant orographic height encircling the domain (i.e., encircling Antarctica) then the form drag will vanish when integrated along it. However, the same integral of the wind stress will not vanish, and therefore must be balanced by something else. To see this explicitly, write the vertically integrated vorticity equation, (21.107), in the form

$$\beta\hat{v} + J(\phi_b, \eta_b) = \text{curl}_z \tilde{\tau}_w - \text{curl}_z \tilde{\tau}_f. \quad (21.108)$$

If we integrate over an area bounded by a contour of constant orographic height (i.e., constant η_b) then both terms on the left-hand side vanish, and the wind stress along that line must be balanced by friction. In the real ocean there may be no such contour that is confined to the ACC — rather, any such contour would meander through the rest of the ocean; indeed, no such confined contour exists in the idealized geometry of Fig. 21.19.

21.7.3 Form Drag and Baroclinic Eddies

How does the momentum put in at the surface by the wind stress make its way to the bottom of the ocean where it may be removed by form drag? We saw in Section 21.6.2 that one mechanism is by way of a mean meridional overturning circulation, with an upper branch in the Ferrel Cell and a lower branch at the level of the sill, with no meridional flow between. However, the presence of baroclinic eddies allows an eddy form drag to pass momentum vertically within the fluid. Let's see how that works.

We model the channel as a finite number of fluid layers, each of constant density and lying one on top of the other — a ‘stacked shallow water’ model, and one equivalent to a model expressed in isopycnal coordinates. The wind provides a stress on the upper layer, which sets it into motion, and this in turn, via the mechanism of form drag, provides a stress to the layer below, and so on until the bottom is reached. The lowest layer then equilibrates via form drag with the bottom topography or via Ekman friction, and the general mechanism is illustrated in Fig. 21.25.

Recalling the results of Section 3.6, the zonal form drag at a layer interface is given by

$$\bar{\tau}_i = -\overline{\eta_i} \frac{\partial p_i}{\partial x} = -\rho_0 f \overline{\eta_i v_i}, \quad (21.109)$$

where p_i is the pressure and η_i is the displacement at the i -th interface (i.e., between the i -th and $(i+1)$ -th layer as in Fig. 21.26), and the overbar denotes a zonal average. If we define the averaged meridional transport in each layer by

$$V_i = \int_{\eta_i}^{\eta_{i-1}} \rho_0 v \, dz, \quad (21.110)$$

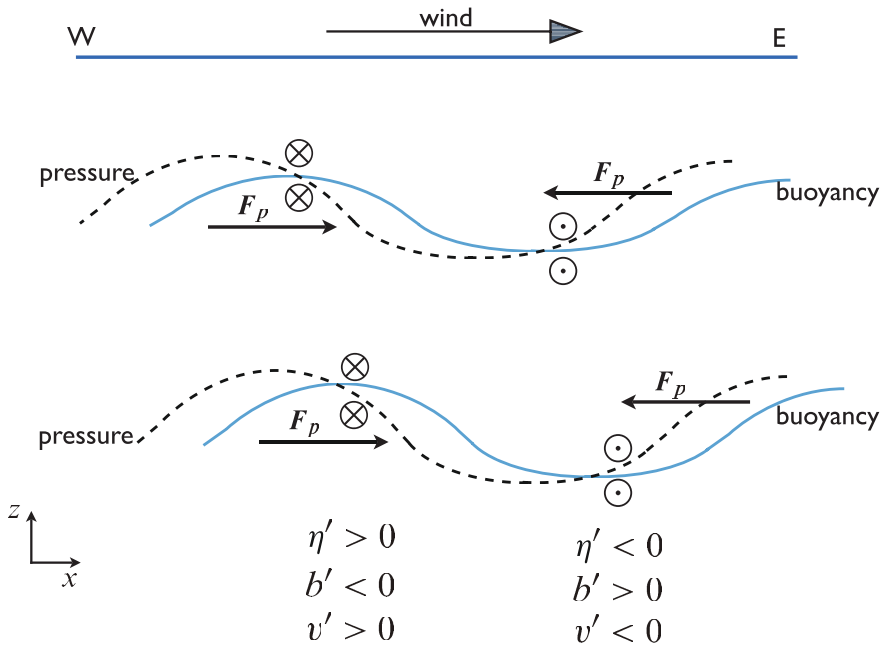


Fig. 21.25 Eddy fluxes and form drag in a Southern Hemisphere channel, viewed from the south. Cold (less buoyant) water flows equatorwards and warm water poleward, so that $\bar{v}'\bar{b}' < 0$. The pressure field (dashed lines) provides a form drag on the successive layers, F_p , shown. At the ocean bottom the westward form drag on the fluid arising through its interaction with the orography is equal and opposite to that of the eastward wind stress at the top. The mass fluxes in each layer are given by $v'h' \approx -\partial_z(v'\bar{b}'/N^2)$. If the magnitude of buoyancy displacement increases with depth then $\bar{v}'\bar{h}' < 0$.

then, neglecting the meridional momentum flux divergence (for reasons given in the next subsection), the time and zonally averaged zonal momentum balance for each layer of fluid are:

$$-f\bar{V}_1 = \tau_w - \tau_1 = \eta_1 \frac{\overline{\partial p_1}}{\partial x} + \tau_w, \quad (21.111a)$$

$$-f\bar{V}_i = \tau_{i-1} - \tau_i = -\eta_{i-1} \frac{\overline{\partial p_{i-1}}}{\partial x} + \eta_i \frac{\overline{\partial p_i}}{\partial x}, \quad (21.111b)$$

$$-f\bar{V}_N = \tau_{N-1} - \tau_N = -\eta_{N-1} \frac{\overline{\partial p_{N-1}}}{\partial x} + \eta_b \frac{\overline{\partial p_b}}{\partial x} - \tau_f, \quad (21.111c)$$

where the subscripts 1, i and N refer to the top layer, an interior layer, and the bottom layer, respectively. Also, η_b is the height of the bottom topography and τ_w is the zonal stress imparted by the wind which, we assume, is confined to the uppermost layer. The term τ_f represents drag at the bottom due to Ekman friction, but we have neglected any other viscous terms or friction between the layers.

The vertically integrated meridional mass transport must vanish, and thus summing over all the layers (21.111) becomes

$$0 = \tau_w - \tau_f - \tau_N, \quad (21.112)$$

or, noting that $\tau_N = -\eta_b \overline{\partial p_b / \partial x}$,

$$\tau_w = \tau_f - \eta_b \frac{\overline{\partial p_b}}{\partial x}. \quad (21.113)$$

Thus, the stress imparted by the wind (τ_w) may be communicated vertically through the fluid by form drag, and ultimately balanced by the sum of the bottom form stress (τ_N) and the bottom friction (τ_f).

Momentum dynamics in height coordinates

We now look at these same dynamics in height coordinates, using the quasi-geostrophic TEM formalism, and it may be helpful to review Section 10.3 before proceeding. As in (10.61), we write the zonally averaged momentum equation in the form

$$-f_0\bar{v}^* = \nabla_m \cdot \mathbf{F} + \frac{\partial \tilde{\tau}}{\partial z}, \quad (21.114)$$

where $\bar{v}^* = \bar{v} - \partial_z(\overline{v'b'}/\bar{b}_z)$ is the residual meridional velocity, $\tilde{\tau}$ is the zonal component of the kinematic stress (wind-induced and frictional, and typically important only in an Ekman layer at the surface and in a frictional layer at the bottom) and \mathbf{F} is the Eliassen–Palm flux, which satisfies

$$\nabla_m \cdot \mathbf{F} = -\frac{\partial}{\partial y} \overline{u'v'} + \frac{\partial}{\partial z} \left(\frac{f_0}{N^2} \overline{v'b'} \right) = \overline{v'q'}. \quad (21.115)$$

Now, if the horizontal velocity and buoyancy perturbations are related by $v' \sim b'/N$ (meaning available potential energy and kinetic energy are roughly similar, see also Section 12.4), then the two terms comprising the potential vorticity flux scale as

$$\frac{\partial}{\partial y} \overline{u'v'} \sim \frac{v'^2}{L_e}, \quad \frac{\partial}{\partial z} \left(f_0 \frac{\overline{v'b'}}{\bar{b}_z} \right) \sim \frac{v'^2}{L_d}, \quad (21.116)$$

where L_e is the scale of the eddies and L_d is the deformation radius. If the former is much larger than the latter, as we might expect in a field of developed geostrophic turbulence (and as is observed in the ACC), then the potential vorticity flux is dominated by the buoyancy flux and (21.114) becomes

$$-f_0\bar{v}^* \approx \frac{\partial \tilde{\tau}}{\partial z} + \frac{\partial}{\partial z} \left(f_0 \frac{\overline{v'b'}}{\bar{b}_z} \right). \quad (21.117)$$

In the ocean interior the frictional terms, $\partial \tilde{\tau} / \partial z$, are small, and (21.117) represents a balance between the Coriolis force on the residual flow and the form stress associated with the vertical component of the EP flux (an association further explained in Section 10.4.3).

If we integrate (21.117) over the depth of the channel the term on the left-hand side vanishes and we have

$$\tilde{\tau}_w = \tilde{\tau}_f - \left[f_0 \frac{\overline{v'b'}}{\bar{b}_z} \right]_{-H}^0, \quad (21.118)$$

where $\tilde{\tau}_w$ is the wind stress and $\tilde{\tau}_f$ is the frictional stress at the bottom (both divided by ρ_0). Equation (21.118) expresses essentially the same momentum balance as (21.113). Thus, the EP flux expresses the passage of momentum vertically through the water column, the momentum being removed at the bottom through frictional stresses and/or form drag with the orography.

Mass fluxes and thermodynamics

Associated with the form drag is a meridional mass flux in each layer, which in the layered model appears as V_i (a thickness flux) in each layer. The satisfaction of the momentum balance at a particular latitude goes hand-in-hand with the satisfaction of the mass balance. Above any topography the Eulerian mean momentum equation is, with quasi-geostrophic scaling and neglecting eddy momentum fluxes,

$$f_0\bar{v} = \frac{\partial \tilde{\tau}}{\partial z}, \quad (21.119)$$

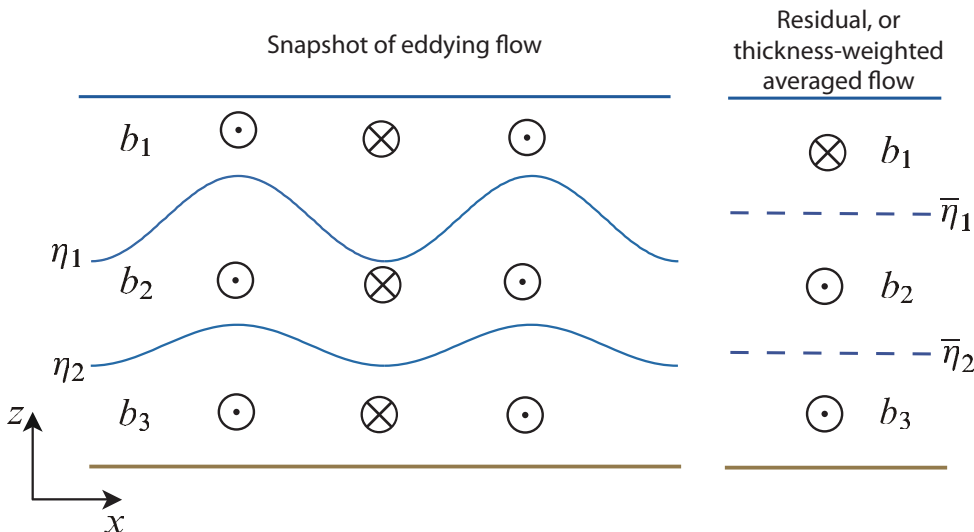


Fig. 21.26 An example of the meridional flow in an eddying channel. The eddying flow may be organized such that, even though at any given level the Eulerian meridional flow may be small, there is a net flow in a given isopycnal layer. The residual (\bar{v}^*) and Eulerian (\bar{v}) flows are related by $\bar{v}^* = \bar{v} + \bar{v}'h'/\bar{h}$; thus, the thickness-weighted average of the eddying flow on the left gives rise to the residual flow on the right, where $\bar{\eta}_i$ denotes the mean elevation of the isopycnal interface η_i .

where \bar{v} is the zonally averaged meridional velocity and $\bar{\tau}$ is the zonal component of the kinematic stress. The zonally averaged meridional flow is thus purely ageostrophic and since the stress, $\bar{\tau}$, is fairly constant in the interior, the mean meridional flow is non-zero only near the surface (i.e., equatorward Ekman flow) and near the ocean bottom, where the flow can be supported by friction and/or form drag. Even in an eddying flow, the Eulerian circulation is primarily confined to the upper Ekman layer and a frictional or topographically interrupted layer at the bottom, as sketched in Fig. 21.27. This is a perfectly acceptable description of the flow, and is not an artifact in any way.

However, and analogously to the atmospheric Ferrel Cell (Sections 14.7 and 15.2.2), if the flow is unsteady this circulation does not necessarily represent the flow of water parcels, nor does it imply that water parcels cross isopycnals, as might be suggested by the dark blue circulation (ψ_{Euler}) in Fig. 21.27. The flow of parcels is better represented by the *residual*, or *thickness-weighted*, flow, and as sketched in Fig. 21.26 and Fig. 21.27 there can be a net meridional residual flow in a given layer (i.e., of a given water mass type) *even when the net meridional Eulerian flow at the level of mean height of the layer is zero*.

The vertically integrated residual mass flux must vanish, and even though one component of this — the equatorward Ekman flow — is determined mechanically, the overall sense of the residual circulation is not determined by the momentum balance alone: thermodynamic effects play a role. The zonally averaged thermodynamic equation may be written in TEM form as

$$\frac{\partial \bar{b}}{\partial t} + J(\psi^*, \bar{b}) = Q_{[b]}, \quad (21.120)$$

where $J(\psi^*, \bar{b}) = (\partial_y \psi^*) (\partial_z b) - (\partial_z \psi^*) (\partial_y b) = \bar{v}^* \partial_y b + \bar{w}^* \partial_z b$, ψ^* is the streamfunction of the residual flow and $Q_{[b]}$ represents heating and cooling, which occur mainly at the surface. In the ocean interior and in a statistically steady state we therefore have

$$J(\psi^*, \bar{b}) = 0, \quad (21.121)$$

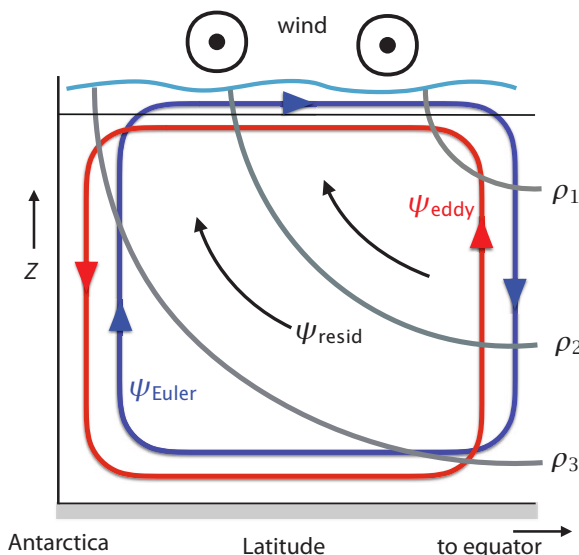


Fig. 21.27 Idealization of the Eulerian, eddy-induced ('bolus'), and residual streamfunctions in a circumpolar channel. The clockwise Eulerian circulation is forced by the eastward winds, the bolus circulation opposes it, and the net, or residual, circulation is nearly along isopycnals.²⁶

the general solution of which is $\psi^* = G(\bar{b})$, where G is an arbitrary function. That is, the interior residual flow is along isopycnals (Fig. 21.27). At the surface, however, the flow is generally not adiabatic, because of heat exchange with the atmosphere, and so the residual flow can be across isopycnals. The sense of the subsurface circulation determines how the form drag varies with depth; if the residual flow were zero, for example, then, either from (21.111) or from (21.117), we see that the form drag must be constant with depth.

21.7.4† An Idealized Adiabatic Model

We finally consider a simple but rather illuminating model of the ACC.²⁷ The simplifying assumption we make is that the flow is adiabatic everywhere; it then follows that the net overturning, as given by the residual circulation, is zero. We can see this by first noting that in a statistically steady state the flow satisfies (21.121), implying that the residual flow is along isopycnals. However, if there is a meridional buoyancy gradient at the surface (where isopycnals outcrop) there can be no surface residual flow (because this would be cross-isopycnal); it then follows that there can be no net flow along isopycnals in the interior, because if these outcrop there would be a net fluid source, and hence diapycnal flow, at the surface. This idealized limit has thus led to the 'vanishing of the Deacon Cell'. In reality the flow is not adiabatic near the surface and the residual flow will not vanish, but it is likely to be weaker than either the Eulerian or the eddy-induced flow (as sketched in Fig. 21.27).

The zonal momentum equation in this limit follows from (21.117), which with $\bar{v}^* = 0$ gives

$$\frac{\partial \tilde{\tau}}{\partial z} \approx -\frac{\partial}{\partial z} \left(f_0 \frac{\overline{v' b'}}{\bar{b}_z} \right). \quad (21.122)$$

The equivalent balance for the Eulerian flow is, using the definition of \bar{v}^* ,

$$-f_0 \bar{v} = \frac{\partial \tilde{\tau}}{\partial z} \quad \rightarrow \quad f_0 \bar{v} = f_0 \frac{\partial}{\partial z} \left(\frac{\overline{v' b'}}{\bar{b}_z} \right). \quad (21.123a,b)$$

These equations represent *dynamical* balances; they do not follow from the momentum equation without making additional assumptions, in this case that $\bar{v}^* = 0$. In the residual equation, (21.122),

the wind stress is balanced by the divergence of the Eliassen–Palm flux, which is dominated by the contribution from the buoyancy flux, and in the ocean interior where the stress is small the meridional buoyancy flux will be constant with height. Equation (21.123b) represents a balance between the Coriolis force on the equatorward flow and form drag. If the frictional stress is small in the interior then the form drag does not vary in the vertical and the right-hand side of (21.123) is small. The zonally averaged meridional flow in the interior is then also small, and the equatorial flow in the top Ekman layer is balanced by a return flow at the bottom of the ocean involving topographic form stress or a bottom Ekman layer.

Integrating (21.122) from the surface (where $\tilde{\tau} = \tilde{\tau}_w$) to a stress-free level in the interior (where $\tilde{\tau} = 0$) gives

$$\tilde{\tau}_w = f_0 \frac{\overline{v' b'}}{\bar{b}_z}, \quad (21.124)$$

if the buoyancy flux at the surface is small. If we are now willing to parameterize the eddy fluxes in terms of the mean flow, then we can predict the stratification. Thus, let $\overline{v' b'} = -\kappa \partial \bar{b} / \partial y$, where κ is an eddy diffusivity, and noting that $s = -\bar{b}_y / \bar{b}_z$ is the slope of the isopycnals, we find

$$\tilde{\tau}_w = \kappa f_0 s = \kappa \frac{f_0^2}{\bar{b}_z} \frac{\partial \bar{u}}{\partial z}, \quad (21.125)$$

where the second equality uses thermal wind balance. Thus, given κ , we can predict the isopycnal slope [$s = \tilde{\tau}_w / (\kappa f_0)$] and, potentially, the total baroclinic transport of the ACC as a function of the wind stress. The sense of the residual circulation can be inferred if the diabatic fluxes at the surface are known, but at the same time these fluxes depend in a complicated way on both the lateral eddy fluxes and the general circulation itself. We come back to this in Sections 21.8 and 21.9.

21.7.5 Form Stress and Ekman Stress at the Ocean Bottom

Earlier, we noted that the stress at the ocean bottom is observed to be dominated by form stress, rather than Ekman friction, in the ACC. A simple scaling argument helps understand why this should be. The form stress scales like

$$\tau_{form} \sim \eta_b \frac{\partial p_b}{\partial x} \sim \eta_b \rho_0 U f, \quad (21.126)$$

where we have used geostrophic balance and U is a scaling for the horizontal velocity. The frictional stress due to an Ekman layer (Section 5.7) scales like

$$\tau_{Ekman} \sim \rho_0 A \frac{\partial u}{\partial z} \sim \frac{\rho_0 A U}{d} \sim \rho_0 d U f, \quad (21.127)$$

where A is the eddy kinematic viscosity and $d = \sqrt{A/f}$ is the Ekman layer thickness. The ratio of these two stresses thus scales as

$$\frac{\tau_{form}}{\tau_{Ekman}} \sim \frac{\eta_b}{d}. \quad (21.128)$$

We therefore expect the form stress to dominate the Ekman stress if the variations in topography are greater than the Ekman layer thickness, and if the flow goes *over* the topography rather than around it. In the ACC the topography is hundreds or even thousands of metres high whereas the bottom Ekman layer may be of order tens of metres, and furthermore the predominantly eastward flow must (unlike the situation in gyre circulations) go *over* the topography. Thus, form stress dominates the frictional, Ekman layer, stress at the bottom of the ACC.

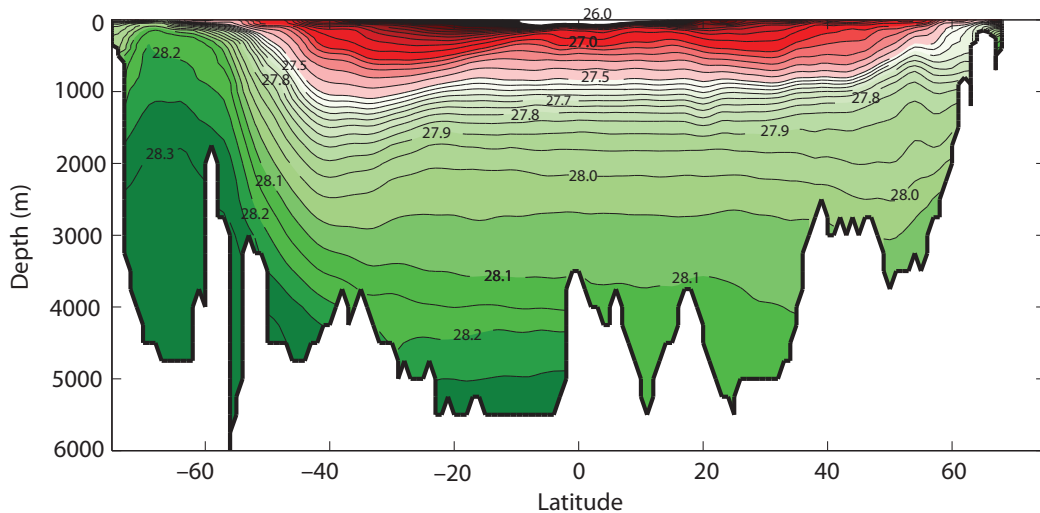


Fig. 21.28 Neutral density in the Atlantic at 25° W from woce. A weakly stratified water mass at mid-depth, roughly between the 28 and 28.1 isopycnals, is associated with the inflow of NADW in the Atlantic Ocean. The contour intervals are 0.1 and 0.05 kg m^{-3} for isopycnals greater and lower than 27.5 kg m^{-3} , coloured green and red, respectively.

21.7.6 Differences Between Gyres and Channels

In the dynamics of the ACC, the wind stress itself seems to play an important role, whereas in our discussion of gyres in chapter 19 the wind stress *curl* was dominant. What is the root of this difference?²⁸ Suppose that we change the wind stress, but not its curl, in a closed basin. The vertically integrated gyral flow, as given for example by the Stommel solution (19.39) or its two-gyre counterpart, does not change at all. However, the vertical structure of this flow will in general change; for example, if the wind is made uniformly more eastward, there will be a corresponding increase in the equatorward flux in the Ekman layer that must return polewards at depth (assuming that the western boundary current balances only the Sverdrup flow). At the same time, the added force from the wind must be balanced by an increased pressure difference between the western and eastern boundaries. This may be achieved if the sea-surface tilts upwards to the east, so producing a net (vertically integrated) poleward geostrophic flow. The subsurface isopycnal slopes may then adjust in order to reduce this flow to near zero in the abyss. The added force provided by the basin walls on the fluid in the basin is a kind of form drag (rather like the force provided by the sill in Section 21.6), and integrated around the basin this force must be equal and opposite to the force supplied by the wind. In contrast, in a channel adding a constant wind produces a direct change in its zonal transport. This is because the wind stress is balanced by form drag and bottom friction, and both of these depend on the zonal flow at the channel bottom.

21.8† A DYNAMICAL MODEL OF THE RESIDUAL OVERTURNING CIRCULATION

In the last section it became clear that the ACC is a region of strongly eddying activity, and one effect of these eddies is to reduce the slope of the isopycnals, so reducing the available potential energy of the flow. Thus, the sketches of Fig. 21.21 and Fig. 21.22 do not properly represent the state of the channel region: not only do the isopycnals slope, but the southward flowing water parcels can enter the channel region above any sill. That is, the zonally averaged *residual* meridional flow can be non-zero, and the deep stratification can be non-zero, even without topography. In this section we seek to build a model that combines our view of the ACC, as described in Section 21.7, with

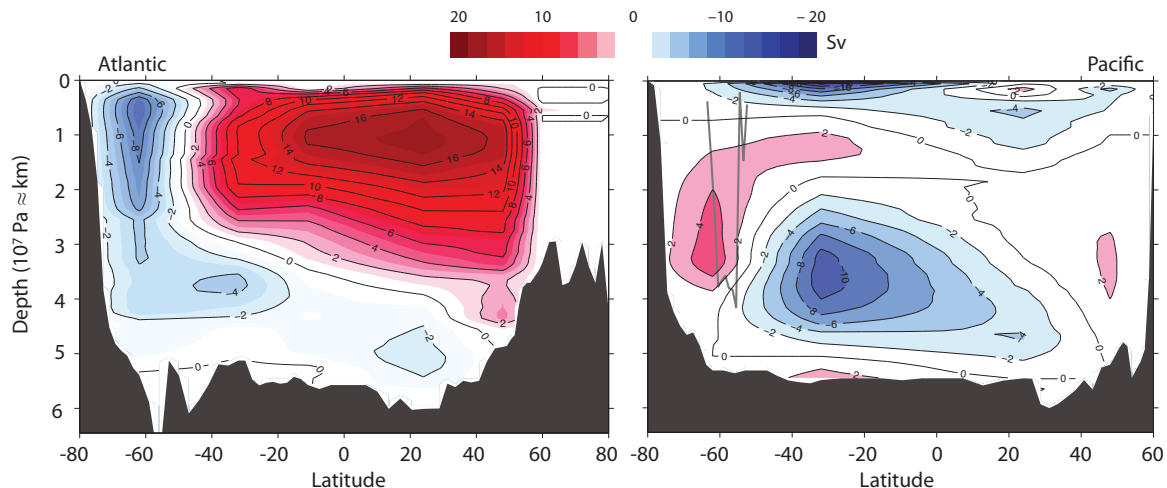


Fig. 21.29 Overturning circulations in the Atlantic and Pacific Oceans as determined by an inverse calculation. South of about 35° the circulation is not a true streamfunction, because of the open boundaries, and this may lead to errors, especially in the Pacific. (See Fig. 21.1 for another Atlantic estimate.)

the view of the partially wind-driven overturning circulation described in Section 21.6. In spite of these additions the model is still incomplete, for it treats only one basin, and it has ad hoc aspects in its treatment of eddy effects.

Our model is partially motivated by the plot of the stratification shown in Fig. 21.28 and the overturning circulations of Fig. 21.29, as abstracted in Fig. 21.30. Although nominally a sketch of the global MOC, of the individual basins it most resembles the circulation of the Atlantic where there are two main circulating masses of water, North Atlantic Deep Water (NADW) and Antarctic Bottom Water (AABW), as seen in Fig. 21.29. The NADW outcrops in high northern latitudes and high southern latitudes, and AABW just at high Southern latitudes. The Pacific overturning circulation (Fig. 21.29) is rather different, for here there is really no mid-depth cell corresponding to NADW; there is essentially *only* a bottom cell of Antarctic bottom water spreading northward. Finally, we note that isopycnals are flat over most of the ocean, but have a fairly uniform slope in the Southern Ocean. (Figure 21.28 shows the Atlantic; the situation is similar for the Pacific.) We will now construct a dynamical model that attempts to describe these features.³⁰

Let us first imagine there is a wall at the equator, and make a model of the circulation in the Southern Hemisphere, that is, essentially of AABW. There's an obvious connection to the Indian Ocean and, if a little less obvious at the moment, to the Pacific.

21.8.1 Model Phenomenology

We divide the basin into two regions, a *Southern Channel* and a *basin*, as in Fig. 21.31 (see also the shaded box on page 850). In the channel the isopycnals slope, and we anticipate a balance between wind effects and baroclinic instability: in the absence of eddies the isopycnals are vertical, as in Fig. 21.21, and baroclinic activity causes the isopycnals to slump. In the basin region we invoke an ansatz that the isopycnals are flat — the model applies below the thermocline where wind effects cause stratification. Wind over the channel induces a northwards Ekman flux, and the return flow occurs at the bottom of the channel, as in the thick arrows in Fig. 21.31, because in the interior the flow is nearly geostrophic and the zonally-averaged geostrophic meridional flow is zero. However, it is the residual circulation that carries water properties and that will connect to the basin flow, and thermodynamic considerations suggest that the flow will circulate along the dashed lines in

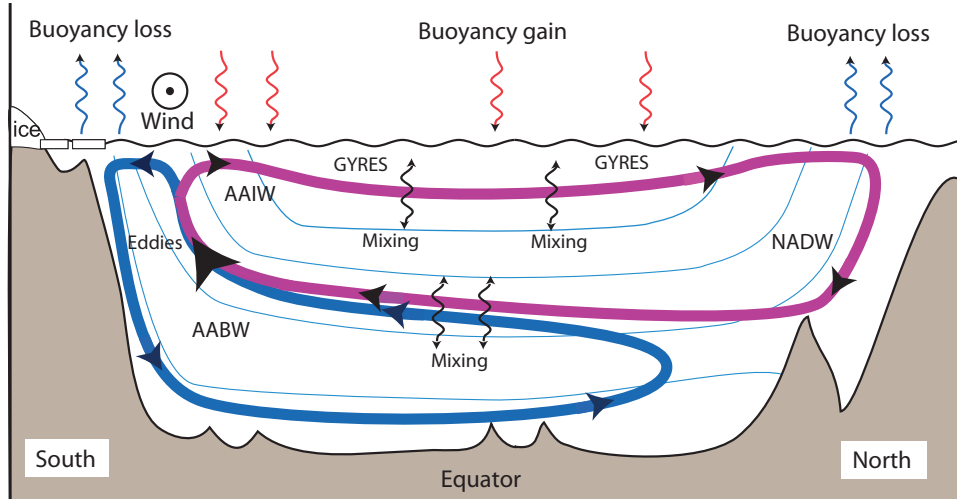


Fig. 21.30 The overturning circulation of the ocean and the main processes that produce it — winds, mixing, baroclinic eddies and surface buoyancy fluxes.²⁹ The sketch is most representative of the Atlantic, which is the major contributor to the global average. Observational views are given in Fig. 21.18 and Fig. 21.29.

Fig. 21.31. In the basin there will be an advective-diffusive balance in the vertical, and the flow will be non-zero only if the diffusivity is non- zero. This flow should connect smoothly to the more adiabatic flow in the channel. Let us see how the equations allow this to be accomplished, and if we can obtain estimates for the strength and structure of the flow.

21.8.2 Equations of Motion

We will use zonally-averaged equations of motion and write them in residual, or TEM, form because the treatment of mesoscale eddies is more convenient and the equations directly predict the velocities that advect the tracers. Thus, following the methodology of Section 10.3, we define a *residual flow* such that

$$\bar{v}^* = \bar{v} - \frac{\partial}{\partial z} \left(\frac{1}{N^2} \overline{v' b'} \right), \quad \bar{w}^* = \bar{w} + \frac{\partial}{\partial y} \left(\frac{1}{N^2} \overline{v' b'} \right), \quad (21.129)$$

where $N^2 = \partial \bar{b} / \partial z$, which is assumed to vary only very slowly. The residual velocities \bar{v}^* and \bar{w}^* more nearly represent the trajectories of fluid parcels than the Eulerian velocities, \bar{v} and \bar{w} . There are no fluxes in the buoyancy equation and only the potential vorticity flux, $\overline{v' q'}$, need be parameterized.

We will further suppose that the large scale flow satisfies planetary-geostrophic scaling, and so we drop the time derivative in the momentum equation and assume the zonal flow is in geostrophic wind balance. Including forcing and dissipation terms, our equations of motion become

$$-f\bar{v}^* = \overline{v' q'} + \frac{\partial \tau}{\partial z}, \quad \frac{\partial \bar{b}}{\partial t} + \bar{v}^* \frac{\partial \bar{b}}{\partial y} + \bar{w}^* \frac{\partial \bar{b}}{\partial z} = \kappa_v \frac{\partial^2 \bar{b}}{\partial z^2}. \quad (21.130a,b)$$

The velocities are non-divergent and may be represented by a streamfunction so that $(\bar{v}^*, \bar{w}^*) = (-\partial \psi / \partial z, \partial \psi / \partial y)$, and we will assume that the residual velocities themselves satisfy the boundary

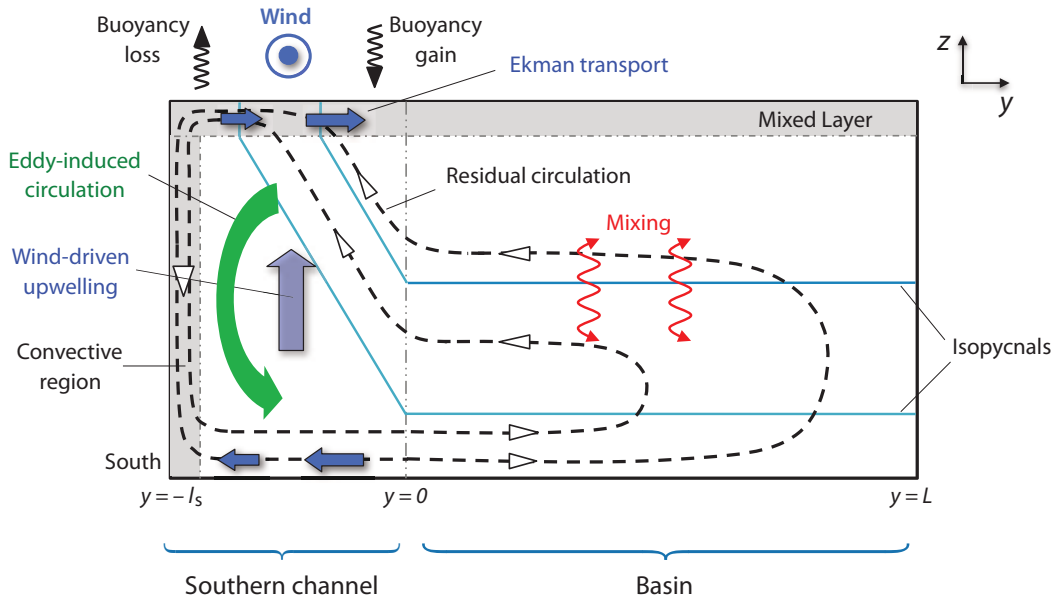


Fig. 21.31 A model of the single hemisphere meridional overturning circulation, crudely representing an idealized Antarctic Bottom Water (AABW) cell. In the Atlantic this cell sits below the interhemispheric North Atlantic Deep Water Cell, but it sits alone in the Pacific and India Oceans. Thin solid lines are the isopycnals, the dashed black line is a residual overturning streamfunction. The thick dark blue arrows are the Eulerian circulation, namely the top and bottom Ekman transport and the wind-driven upwelling.

conditions of no normal flow. The zonal wind, \bar{u} , may be obtained from thermal wind balance, $f\partial\bar{u}/\partial z = -\partial\bar{b}/\partial y$, and the stress, τ , is only non-zero near the top (wind-stress) and bottom (Ekman drag). We will henceforth drop the $*$ notation, and all variables are understood to be residuals and zonal averages. These equations apply in both the channel and basin regions, but with different dominant balances.

Equations in the channel

The right-hand side of (21.130a) contains the eddy flux of potential vorticity which we parameterize using an eddy diffusivity,

$$\overline{v'q'} = -K_e \frac{\partial \bar{q}}{\partial y}, \quad (21.131)$$

where K_e is the eddy diffusivity. (It is more-or-less a ‘Gent–McWilliams’ coefficient, as in Section 13.6.) The Coriolis parameter is almost constant in the channel, and we denote it f_s . For the large-scale ocean the potential vorticity is given by

$$\bar{q} \approx f_s \frac{\partial}{\partial z} \left(\frac{\bar{b}}{\bar{b}_z} \right), \quad \text{so that} \quad \frac{\partial \bar{q}}{\partial y} \approx f_s \frac{\partial}{\partial z} \left(\frac{\bar{b}_y}{\bar{b}_z} \right) = -f_s \frac{\partial S}{\partial z}, \quad (21.132)$$

where $S = -\bar{b}_y/\bar{b}_z$ is the slope of the isopycnals (and the similarity with the Gent–McWilliams scheme is now clear). The potential vorticity flux is then given by

$$\overline{v'q'} \approx f_s K_e \frac{\partial S}{\partial z}, \quad (21.133)$$

and the momentum equation becomes

$$-f_S \bar{v} = f_S K_e \frac{\partial S_b}{\partial z} + \frac{\partial \tau}{\partial z}. \quad (21.134)$$

Since $\bar{v}^* = -\partial \psi / \partial z$ we integrate this from the top to a level z and obtain

$$\psi = -\frac{\tau_w}{f_S} + K_e S, \quad (21.135)$$

where both f_S and S are negative and τ_w is the surface kinematic stress in the channel. We have assumed $\psi = 0$, $S = 0$ at the surface (the base of the mixed layer) and $\tau = 0$ in the interior.

The buoyancy equation in terms of streamfunction is

$$\bar{v} \cdot \nabla \bar{b} = \kappa_v \frac{\partial^2 \bar{b}}{\partial z^2} \quad \text{or} \quad \frac{\partial \psi}{\partial y} \frac{\partial \bar{b}}{\partial z} - \frac{\partial \psi}{\partial z} \frac{\partial \bar{b}}{\partial y} = \kappa_v \frac{\partial^2 \bar{b}}{\partial z^2}, \quad (21.136)$$

which can be written as

$$\frac{\partial \psi}{\partial y} + S \frac{\partial \psi}{\partial z} = \kappa_v \frac{\partial^2 \bar{b}}{\partial z^2}. \quad (21.137)$$

The boundary condition on ψ for this equation will be supplied by the basin! The other boundary condition we will need is the buoyancy distribution at the top, and so we specify

$$\bar{b}(y, z = 0) = b_0(y). \quad (21.138)$$

Equations in the basin

In the basin the slope of the isopycnals is assumed zero and (21.137) becomes the conventional upwelling diffusive balance,

$$w \frac{\partial \bar{b}}{\partial z} = \kappa \frac{\partial^2 \bar{b}}{\partial z^2} \quad \text{or} \quad \frac{\partial \psi}{\partial y} \frac{\partial \bar{b}}{\partial z} = \kappa_v \frac{\partial^2 \bar{b}}{\partial z^2}. \quad (21.139)$$

If we integrate this from the edge of the channel, $y = 0$, to the northern edge, $y = L$, we obtain

$$\psi|_{y=0} = -\kappa_v L \frac{\bar{b}_{zz}}{\bar{b}_z}. \quad (21.140)$$

This equation then becomes the needed boundary condition for the equations in the channel.

21.8.3 Scaling

The above equations do not give up analytic solutions, but we can use them to obtain estimates of the flow strength and structure. Let us scale the equations by letting

$$z = h\hat{z}, \quad y = l\hat{y}, \quad \tau_S = \tau_0 \hat{\tau}_S, \quad f_S = \bar{f}_S \hat{f}, \quad \psi = \frac{\tau_0}{f_S} \hat{\psi}, \quad S = \frac{h}{l} \hat{S}, \quad (21.141)$$

where $\bar{f}_S = |f_S|$, a hat denotes a nondimensional value and h is a characteristic vertical scale such that $S \sim h/l$, and *this will emerge as part of the solution*.

A Model of the Meridional Overturning Circulation

The essential features of the model of the MOC of Sections 21.8 and 21.9 are:

Formulation

- The model is zonally averaged, in a single basin, with simple geometry: a zonally re-entrant channel at high latitudes, with an enclosed basin between it and the northern boundary. The effects of wind-driven gyres are neglected; the dynamics in the enclosed basin can be regarded as being below the main thermocline.
- The equations solved are the planetary geostrophic equations, in a transformed Eulerian mean form, with the effects of mesoscale eddies being parameterized with a simple down-gradient buoyancy flux scheme in the momentum equation.
- The ocean is divided into three regions: a northern convective region, a cross-equatorial basin region, and a southern channel.
- The dynamics are treated separately in these three regions, and the solutions matched at the boundaries:
 - (i) In the southern channel there is a balance between wind stress (causing isopycnals to steepen) and the mesoscale eddies, which have a flattening effect. Buoyancy satisfies the full nonlinear advective-diffusive equation.
 - (ii) In the basin region the isopycnals are assumed flat, and by integrating meridionally over the basin this region essentially becomes a boundary condition for the southern channel. The buoyancy equation reduces to a vertical advective-diffusive balance ($w \partial b / \partial z = \kappa \partial^2 b / \partial z^2$).
 - (iii) In the northern convective region the isopycnals are vertical, descending sufficiently far down to connect to the corresponding horizontal isopycnals of the basin. If the northern region is too warm to allow this, the basin isopycnals will extend all the way to the northern boundary.

Properties and Predictions

- If the surface boundary conditions on buoyancy permit, there is an isopycnal pathway from the northern convective region to the southern channel. For small values of diffusivity flow can then circulate, largely adiabatically, from high northern latitudes to high southern latitudes, mechanically pumped by the wind over the southern channel. This may roughly correspond to flow in the Atlantic.
- If the boundary conditions are such that the surface of the northern region is too buoyant, then there is no interhemispheric wind-driven mid-depth circulation and no northern convection, roughly corresponding to flow in the Pacific and Indian Ocean.
- For large values of diffusivity, the flow sinks at high latitudes and upwells in low latitudes, as in a conventional buoyancy/mixing-driven circulation.
- Beneath the wind-driven mid-depth cell, a diffusive cell corresponding to Antarctic Bottom Water forms. Its strength is determined by the diapycnal diffusivity and surface meridional buoyancy gradients.
- The southern channel there is convection at the southern end and elsewhere the isopycnal slope is determined by a balance between wind forcing and eddy effects.
- The effects of mesoscale eddies are parameterized by an eddy diffusivity, but the overall model framework is not fundamentally dependent on that.
- The model cannot account for inter-basin pathways of water, for example between the Atlantic and Pacific Oceans.

If we have scaled properly then variables with hats on are of order one. The nondimensional equations of motion are then

$$\text{Buoyancy evolution: } \partial_{\hat{y}} \hat{\psi} + \hat{S} \partial_{\hat{z}} \hat{\psi} = \epsilon \left(\frac{l}{L} \right) \frac{\partial_{\hat{z}\hat{z}} \hat{b}}{\partial_{\hat{z}} \hat{b}}, \quad (21.142a)$$

$$\text{Momentum balance: } \hat{\psi} = -\frac{\hat{\tau}_S}{\hat{f}} + \Lambda \hat{S}, \quad (21.142b)$$

$$\text{Boundary condition: } \hat{\psi}|_{\hat{y}=0} = -\epsilon \frac{\partial_{\hat{z}\hat{z}} \hat{b}}{\partial_{\hat{z}} \hat{b}}, \quad (21.142c)$$

where

$$\Lambda = \frac{\text{Eddies}}{\text{Wind}} = \frac{K_e}{\tau_0/\bar{f}_S} \frac{h}{l}, \quad \epsilon = \frac{\text{Mixing}}{\text{Wind}} = \frac{\kappa_v}{\tau_0/\bar{f}_S} \frac{L}{h}. \quad (21.143a,b)$$

These are two important nondimensional numbers, and we can obtain estimates of their values by using some observed values for the other parameters. Let us take

$$\begin{aligned} h &= 1 \text{ km}, \quad \kappa_v = 10^{-5} \text{ m}^2 \text{s}^{-1}, \quad K_e = 10^3 \text{ m}^2 \text{s}^{-1}, \quad \rho_0 = 10^3 \text{ kg m}^{-3}, \\ \tau_0 &= 0.1 \text{ N m}^{-2}/\rho_0 = 10^{-4} \text{ N m kg}^{-1}, \quad \bar{f}_S = 10^{-4} \text{ s}^{-1}, \quad L = 10 000 \text{ km}, \quad l_s = 1000 \text{ km}, \end{aligned} \quad (21.144)$$

and we find

$$\Lambda \approx 1, \quad \epsilon \approx 0.1. \quad (21.145)$$

These values come with large error bars: the diffusivity, κ_v , may be much larger in the abyss, and the eddy coefficient K_e is very poorly constrained (indeed, it is a property of the flow itself, not the fluid). Finally, note that Λ and ϵ are not independent of each other for they both depend on the vertical scale of stratification, h , which is a part of the solution. To obtain some theoretical estimates of h we look at some limiting cases.

The small diffusion limit

Suppose that mixing is small and that $\epsilon \ll 1$. We can then *require* that $\Lambda = 1$ in order that the eddy-induced circulation nearly balance the wind-driven circulation (because the diffusive term is small), whence the vertical scale h is given by

$$\frac{h}{l} = \frac{\tau_0/f_S}{K_e}. \quad (21.146)$$

As K_e diminishes h becomes larger, meaning that the isopycnals are near vertical. Using (21.146) in (21.143b) gives

$$\epsilon = \frac{\kappa_v K_e}{(\tau_0/f_S)^2} \frac{L}{l}. \quad (21.147)$$

This is an appropriate nondimensional measure of the strength of the diapycnal diffusion in the ocean. Using (21.142c) we see that $\hat{\psi} \sim \epsilon$ so that the dimensional strength of the circulation goes as

$$\Psi = \epsilon \frac{\tau_0}{f_0} = \kappa_v \frac{K_e}{\tau_0/f_S} \frac{L}{l}. \quad (21.148)$$

Another way to obtain this is to use the fact that for weak diffusion the balance in the dimensional momentum equation is between wind forcing and eddy effects (because they must nearly cancel) so that

$$\frac{\tau_w}{f} \sim K_e S, \quad \text{or equivalently} \quad \frac{h}{l} \sim \frac{\tau_w}{K_e f_s}. \quad (21.149a,b)$$

Advection-diffusive balance in the basin gives

$$\frac{\partial \psi}{\partial y} \frac{\partial \bar{b}}{\partial z} = \kappa_v \frac{\partial^2 \bar{b}}{\partial z^2} \quad \text{whence} \quad \Psi = \frac{\kappa_v L}{h} \quad (21.150a,b)$$

and (21.149b) and (21.150b) together give (21.148).

The high diffusion limit

To explore the high diffusion limit we take $\epsilon \gg 1$. The nondimensional strength of the circulation is given by

$$\hat{\psi} = \mathcal{O}(\epsilon) \gg 1. \quad (21.151)$$

The circulation is now ‘strong’, since $\hat{\psi} \neq \mathcal{O}(1)$. Dimensionally we still have that

$$\Psi = \epsilon \frac{\tau_0}{f_s} \quad \text{or} \quad \Psi = \frac{\kappa_v L}{h} \quad (21.152a,b)$$

but h and ϵ will be different than in the low diffusion limit. Now, if $\hat{\psi} \sim \epsilon \gg 1$ the diffusion driven circulation in the basin cannot be matched by a purely wind-driven circulation in the channel, since the latter is $\mathcal{O}(1)$. Put more physically, as we increase diffusivity the circulation increases in strength, but this cannot connect smoothly to the flow in the channel unless the eddy-driven circulation changes, because the wind-driven circulation is externally fixed. We thus match the basin circulation to an eddy-driven channel circulation and require $\Lambda = \mathcal{O}(\epsilon)$. In particular, if we set $\Lambda = \epsilon$ then

$$\epsilon = \Lambda = \sqrt{\frac{K_e \kappa_v L}{(\tau_0/f_s)^2 l}}. \quad (21.153)$$

This is the square root of the expression for ϵ in the weak diffusion limit. Using (21.153) and (21.152a) we find

$$\frac{h}{l} = \sqrt{\frac{\kappa_v L}{K_e l}}, \quad \Psi = \sqrt{\frac{K_e \kappa_v L}{l}}. \quad (21.154a,b)$$

These are expressions for the characteristic depth and strength of the circulation in a strong mixing regime.

Meaning of the limits

If diffusion is weak the stratification is set by a trade-off between the eddies and wind and this determines h , as in (21.146), and this does not involve diapycnal diffusion at all. However, the strength of the circulation is determined by an upwelling-diffusion balance which gives the estimate $\psi \sim \kappa_v L/h$. Since h is independent of diffusivity we obtain a circulation strength that is linearly proportional to diffusivity, as in (21.148). Since diffusion is, in this limit, small then the circulation is weak, even in the southern channel. The weakness arises because there is a cancellation between the wind stress and eddy terms in (21.135), and a total cancellation would lead to the so-called ‘vanishing of the Deacon Cell — the Deacon Cell here being the residual overturning in the southern channel. It is interesting that the circulation gets weaker as the wind gets stronger;

this counter-intuitive effect arises because the wind steepens the isopycnals and deepens the stratification, so that the diffusive term ($\kappa_v \bar{b}_{zz}$) in the basin gets smaller. From an asymptotic perspective, in the small ϵ limit the residual circulation is zero to lowest order, and at the next order the flow is parallel to the isopycnals in the channel (except in the mixed layer). We will see in the next section that the Deacon cell need not vanish, even in the limit of weak diffusion, if there is a northern source of water.

In the strong diffusion case the diffusivity itself directly affects the stratification, and consequently we get a weaker dependence of the circulation strength on κ_v . In this limit diapycnal mixing deepens the isopycnals in the basin away from the channel, and this deepening in turn means that the diffusion has a weaker effect. Thus, although the circulation is stronger than in the weak diffusion case it has a weaker dependence on diffusivity, to the one half power in fact (21.154b). The second consequence of the deepening is that the isopycnals are steeper in the channel, with the steepening being balanced by the enhanced slumping effects of baroclinic instability, with the wind then only having a secondary effect.

Finally, instead of varying diffusivity we can think of the wind changing. In the weak wind limit the circulation is diffusively driven and independent of the wind strength, as in (21.154b). In the strong wind limit the circulation, as noted above, actually decreases as the wind increases, but still remains proportional to the diapycnal diffusivity κ_v .

21.9† A MODEL OF THE INTERHEMISPHERIC CIRCULATION

We now introduce another ‘water mass’ into the mix — *North Atlantic Deep Water*, or NADW. We thus divide the ocean into three regions as sketched in Fig. 21.32, namely:

- (i) a southern channel (south of about 50° S) where, as before, we expect a balance between eddy effects and wind effects;
- (ii) a basin region (from about 50° S to, say, 60° N), where the isopycnals are fairly flat;
- (iii) a northern convective region (north of 60° N) in which convection produces vertical isopycnals that connect with those in the basin.

Although the dynamics of all three regions are locally different, they must act in concert to produce a dynamically consistent circulation. The main difference, and it is an important one, between this model and the previous one is the presence of an interhemispheric cell that, we will find, is primarily wind driven, and that (for realistic parameter values) sits on top of the lower cell. In the presentation that follows we focus our description on the northern convective region and the upper cell, for the dynamics of the lower cell are very similar to those of the previous section. Further, we seek only scaling relations rather than full analytic or semi-analytic solutions.³¹ We use lower case letters (e.g., h , ψ) to denote field variables and upper case symbols (e.g., H , Ψ) for representative values.

21.9.1 Model Phenomenology

The upper cell has similar characteristics to the wind-driven cell sketched in Fig. 21.22, but we now require the flow in the basin to connect smoothly to an eddy-rich southern channel region, in a similar manner to that described in the previous section. We also suppose that in the northern region the interior flow connects to the surface by way of convection. To see how this occurs, consider a given isopycnal, b_0 say, that outcrops at the surface in the southern channel, slopes down in the channel and becomes horizontal in the basin. If the surface values of b in the northern convective region are all larger (warmer) than b_0 then the isopycnal never outcrops in the north; rather, it continues northward until it intersects the northern wall. If, on the other hand, at some latitude there is a latitude, y_n , say, at which the surface values become lower than b_0 convection will occur and the b_0 isopycnal becomes vertical. There is then an isopycnal pathway from the surface

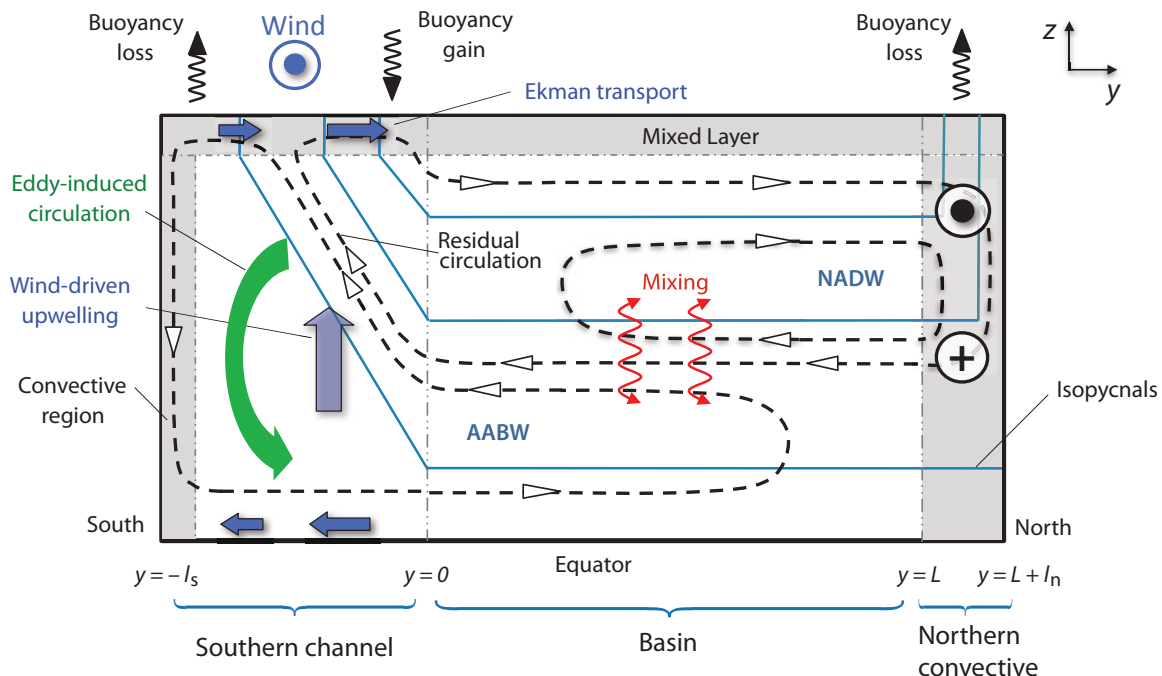


Fig. 21.32 An idealized interhemispheric MOC in a single basin, crudely representing a zonally-averaged Atlantic circulation. The solid blue lines are the isopycnals, the dashed lines with arrows are the streamlines, the dashed vertical lines are the boundaries between adjacent regions, shaded grey areas are the convective regions at high latitudes and the surface mixed layer, and the red curly arrows represent mixing giving a downward diffusive heat flux.

at y_n through the interior to the southern channel. A parcel of water may move along this pathway even in the absence of diffusion; that is, there can be an interhemispheric mid-depth adiabatic circulation.³² Below this cell (which we associate with NADW) there can be a bottom cell of AABW that is diffusively driven, as in the previous section.

21.9.2 Dynamics in the Northern Convective Region

In the northern region (denoted with a subscript N) the values of buoyancy at the surface (i.e., $b_N(y, z = 0)$) are mapped on to the flat isopycnals, $b_B(z)$ in the interior basin region (denoted with a subscript B), and the simplest assumption to make is that the matching occurs by convection. That is, the surface waters convect downward to the level of neutral buoyancy, producing vertical isopycnals ($\partial b_N / \partial z = 0$), and then flow meridionally. By thermal wind the vertical isopycnals give rise to a zonal flow, with the total zonal transport being determined by the meridional temperature gradient and the depth, h , to which flow convects. The zonal flow is thus

$$u_N(y, z) = -\frac{1}{f} \int_{-h}^z \frac{\partial b_N}{\partial y} dz' + \text{constant}, \quad (21.155)$$

where the constant is determined by the requirement that $\int_{-h}^0 u_N dz = 0$, and there are boundary layers in both east and west to bring the flow to zero. When the relatively shallow eastward moving zonal flow collides with the eastern wall it subducts and returns, as sketched in Fig. 21.33, and when the flow reaches the western wall it then moves equatorward in the deep western boundary current. Similarly, it is the upper, northward moving branch of the western boundary current that feeds the

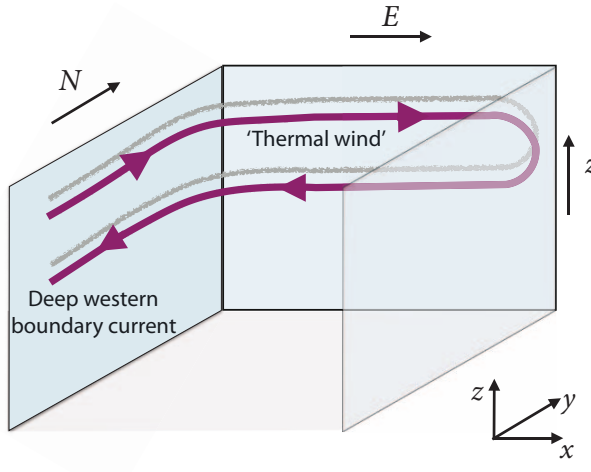


Fig. 21.33 The envisioned mean flow in the northern region of the model of Fig. 21.32. The north–south temperature gradient induces a zonal ‘thermal wind’, which is supplied by and feeds the deep western boundary current, as shown.

eastward moving flow. The total volume transport ($\text{m}^3 \text{s}^{-1}$) in these thermally-induced zonal flows thus translates to a meridional streamfunction given by

$$\int_{x_W}^{x_E} \psi_N \, dx = \int_{-h}^z dz' \int_L^{L_n} u_N \, dy, \quad (21.156)$$

where L_x is the zonal extent of the region, L is the latitude of the southern edge of the convecting region and $L_n = L + l_n$ is the northern edge of the domain (see Fig. 21.32). Using (21.155) gives an estimate for the value of this streamfunction as

$$\Psi_N = \frac{\Delta b H^2}{L_x f_N}, \quad (21.157)$$

where Δb is the surface buoyancy difference across the northern convective region, which in the theory we are describing is an external parameter, and f_N is the Coriolis parameter in the northern region. The streamfunction ψ_N is function of space and Ψ_N is a representative value of it, and H is a representative value of h , the depth to which the convection reaches and so of the stratification.

21.9.3 Connection to Other Regions

In the basin region we posit flat isopycnals and an upwelling diffusive balance, whence

$$w_B \frac{\partial b}{\partial z} = \kappa_v \frac{\partial^2 b}{\partial z^2} \quad \text{giving} \quad \frac{\Psi_B}{L_y} = \frac{\Psi_N - \Psi_S}{L_y} = \frac{\kappa_v}{H}. \quad (21.158)$$

In the channel region the residual circulation arises from a balance between the wind and eddy effects and is given by (21.135), which we can write as

$$\Psi_S = \left(\frac{\tau_0}{f_S} - K_e \frac{H}{l_s} \right), \quad (21.159)$$

with $\bar{f}_S = |f_S|$ as before. Collecting the various expressions above for streamfunction we have

$$\Psi_S = \left(\frac{\tau_0}{f_S} - K_e \frac{H}{l_s} \right), \quad \Psi_N - \Psi_S = \frac{\kappa_v}{H} L_y, \quad \Psi_N = \frac{\Delta b H^2}{f_N L_x}, \quad (21.160a,b,c)$$

with unknowns Ψ_S , Ψ_N and H . The various parameters have approximate values as given in (21.144) as well as

$$L_x = 5000 \text{ km}, \quad L_y = 10000 \text{ km}, \quad \Delta b = 10^{-2} \text{ m s}^{-2}, \quad f_N = 10^{-4} \text{ s}^{-1}. \quad (21.161)$$

Equation (21.160) may be reduced to

$$\frac{\Delta b H^2}{f_N} - \left(\frac{\tau_0}{f_S} - K_e \frac{H}{l_s} \right) L_x = \frac{\kappa_v}{H} L_x L_y, \quad (21.162)$$

which is a cubic equation for the characteristic depth, H , of the upper, NADW, cell in Fig. 21.32. Although there are analytic solutions to cubic equations it is more instructive to consider limiting cases, first with either the northern region or the southern channel absent and then with low or high diffusivity.

No northern source

Suppose that $\Delta b = 0$ and that there is no deep water formation in the north. If κ_v is small then we obtain $H/l_s = (\tau_0/f_S)/K_e$ a, equivalent to (21.146), and $\Psi_S = \Psi_B = 0$. If κ_v is large then we find

$$H^2 = \frac{\kappa_v L l_s}{K_e}, \quad (21.163)$$

so recovering (21.154a). Thus, the dynamics are essentially those of Section 21.8, and there is a single deep, and rather weak, diffusively-driven, cell. The same situation arises if the northern region is too buoyant (e.g., too warm) for then there is no isopycnal pathway between high northern hemispheres and the southern channel, and deep convection does not occur. This case may have relevance to the Pacific Ocean, where the surface at high northern latitudes is insufficiently dense and there is no Pacific equivalent of NADW.

No southern channel

If there is no southern channel then $\Psi_S = 0$ and we have

$$\frac{\Delta b H^2}{f_N} = \frac{\kappa_v}{H} L_x L_y, \quad (21.164)$$

giving

$$H^3 = \kappa_v \left(\frac{f_N L_x L_y}{\Delta b} \right) \quad \text{and} \quad \Psi_N = \Psi_B = (\kappa_v L_y)^{2/3} \left(\frac{\Delta b}{L_x f_N} \right)^{1/3}. \quad (21.165)$$

These are the classical expressions for the thickness of a diffusive thermocline and the strength of a diffusively-driven overturning circulation, essentially as obtained in Sections 21.2.5 and 20.5.1.

Let us now look at the case with all three regions, in the limits of weak and strong diffusivity.

Low diffusivity limit

In this case the upwelling is weak and $|\Psi_N| \approx |\Psi_S|$ and

$$\frac{\Delta b H^2}{f_N} - \left(\frac{\tau_0}{f_S} - K_e \frac{H}{l_s} \right) L_x = 0. \quad (21.166)$$

In this case the basin is just a ‘pass-through’ region: water formed in the North Atlantic just passes through the basin without change, and upwells in the Southern Ocean. For the above expression

to be physical, τ_0 must be non-zero; this requirement is a manifestation of Sandström's effect, that in the absence of diffusivity a mechanical forcing is needed, and if $\tau_0 = 0$ in the above then the only physical solution is $H = 0$.

If we assume that K_e is small then we obtain

$$H = \left(\frac{\tau_0 f_N L_x}{\bar{f}_S \Delta b} \right)^{1/2}, \quad \Psi_S = \Psi_N = \frac{\tau_0 L_x}{\bar{f}_S}, \quad (21.167)$$

which with the parameters chosen earlier gives $H \sim 320$ m and $\Psi \sim 10$ Sv. The residual circulation *does not vanish in the limit of small diffusivity*; rather, it is wind driven, adiabatic, interhemispheric and independent of diffusivity. This is to be contrasted with the case in which deep waters are not produced in the north, as observed in the Pacific Ocean, where in the low diffusivity limit the eddy-induced circulation nearly cancels the wind-driven circulation resulting in small residual circulation, dependent on that diffusivity.

In the more general case we solve (21.166) to give

$$H = \left(\frac{\tau_0 f_N L_x}{\bar{f}_S \Delta b} \right)^{1/2} (-\alpha + \sqrt{1 + \alpha^2}), \quad (21.168)$$

where α is a nondimensional number giving the ratio of eddy to wind effects,

$$\alpha = \frac{1}{2} \frac{K_e}{l_s} \left(\frac{L_x \bar{f}_S f_N}{\tau_0 \Delta b} \right)^{1/2} = \frac{1}{2} \frac{\Psi_{eddy}}{\Psi_{wind}}, \quad (21.169)$$

where

$$\Psi_{wind} = \frac{\tau_0}{\bar{f}_S} \quad \text{and} \quad \Psi_{eddy} = \frac{K_e}{l_s} \left(\frac{\tau_0 f_N L_x}{\bar{f}_S \Delta b} \right)^{1/2}. \quad (21.170)$$

Putting in values from (21.144) and (21.161) gives $\alpha \sim 0.1$, $\Psi_{eddy} \sim 1.6$ Sv and $\Psi_{wind} \sim 10$ Sv, suggesting that wind effects are dominant, but there is considerable uncertainty because K_e is ill-defined and does not have a definitive value.

High diffusivity limit

In the high diffusivity limit the wind-driven upwelling in the Southern Hemisphere is small compared to the mixing-driven upwelling in the ocean basin, and although it seems to be not relevant for today's circulation it may have been important in glacial climates. Equation (21.162) simply becomes (21.164), which as already noted gives us the classical scaling for a diffusively-driven circulation. The upper cell thus fades out before reaching the southern channel but there remains a lower, AABW, cell that connects to the flow in the southern channel as described in Section 21.8.

21.9.4 Final Remarks and Relevance to the Ocean

Over the last several pages we've described a conceptual, but quantitative, theoretical model of the overturning circulation in the ocean. Aside from its idealizations (e.g, simplified geometry), the model has two main shortcomings: it uses an eddy-diffusivity parameterization for the effects of mesoscale eddies, and it treats the ocean one basin at a time. Putting these aside, what does the model tell us?

In the limit of weak diapycnal mixing, which seems relevant to the present mid-depth ocean, and with a northern source of deep water, then the model produces a circulation relevant to the

Atlantic — Fig. 21.32 is an idealization of the Atlantic panel in Fig. 21.29. The strength of the mid-depth overturning circulation is then largely determined by the Ekman transport in the Southern Ocean and, secondarily, eddy effects. The rest of the ocean is essentially forced to adjust and produce the amount of deep water demanded by the Ekman transport and the associated wind-driven upwelling in the Southern Ocean. Beneath this mechanically-forced mid-depth cell lies a diffusively-driven deep cell, and this is the model representation of AABW.

The Pacific Ocean is insufficiently dense at high northern latitudes to produce deep water — compared to the Atlantic it is relatively fresh. That is, there is no isopycnal pathway from the surface waters at high latitudes to the southern channel; and consequently there is no wind-driven mid-depth cell comparable to that of the Atlantic. The model then produces a circulation similar to that of Fig. 21.31, where the northern wall is at a high latitudes in the Northern Hemisphere, and this is an idealization of the Pacific panel in Fig. 21.29. Since the diffusivity is weak the circulation is weak, particularly in the Northern Hemisphere. The flow in the world's ocean is much more interconnected than these simple ideas suggest, and in reality the flow travels from basin-to-basin on what has been metaphorically called a conveyor belt.³³ But our own story ends here, for now. How the models above might be extended to produce a global flow is a chapter for another day.

Notes

- 1 Warren (1981) provides a review and historical background and Schmitz (1995) surveys the observations and provides an interpretation of the deep global circulation. Marshall & Speer (2012) review the role of the Southern Ocean.
- 2 The word 'driven' is fraught with ambiguity, even when the subject matter is well understood. Does it refer to the proximate mechanical forces producing the motion, or to the controlling device? The former (which is quite common in physical science) suggests that an engine drives a car, for that is what makes the wheels go round, whereas the latter suggests that, in fact, the driver drives the car. For the less well-understood ocean there is scope for still more confusion, and the context in which the word is used becomes important. What we in this chapter sometimes call buoyancy-driven might be better called mixing-driven, since it is the mixing of fluid parcels that makes potential energy available for the circulation. *Caveat lector.*
- 3 Adapted from Wunsch (2002). The figure shows a 'state estimate' — a combination of models and observation, similar to an atmospheric reanalysis.
- 4 Figure kindly prepared by Neven Stjepan Fućkar, using the climatology of Conkright *et al.* (2001).
- 5 As in Haney (1971). The value of C , which is not necessarily related to that of κ , is often taken to be such that the heat flux is of order $30 \text{ W m}^{-2} \text{ K}^{-1}$, but it is certainly not a universal constant.
- 6 Adapted from Paparella & Young (2002).
- 7 Rossby (1965).
- 8 Adapted from Ilicak & Vallis (2012).
- 9 I am grateful to Tom Haine for pointing out this argument. See also Haine & Marshall (1998) and Hughes & Griffiths (2008).
- 10 Ocean convection is also reviewed by Marshall & Schott (1999).
- 11 Sandström (1908, 1916). Sandström's discussion was rather qualitative and generally thermodynamic in nature, with friction playing only an implicit role. Since then a number of related statements with varying degrees of generality and precision have been given (e.g., Dutton 1986, Huang 1999, Paparella & Young 2002). Section 21.2.3 follows Paparella and Young.
- 12 The original box model is due to Stommel (1961), and many studies with variations around this have followed. Rooth (1982) developed the idea of a buoyancy-driven pole-to-pole overturning circulation, and Welander (1986) discussed, among other things, the role of boundary conditions on temperature and salinity at the ocean surface. Thual & McWilliams (1992) systematically explored how box models compare with two-dimensional fluid models of sideways convection, Quon & Ghil

- (1992) explored how multiple equilibria arise in related fluid models, and Dewar & Huang (1995) discussed the problem of flow in loops. Cessi & Young (1992) tried to derive simple models systematically from the equations of motion, obtaining various nonlinear amplitude equations. Our discussion is just a fraction of all this — see also Whitehead (1995) and Cessi (2001) for reviews.
- 13 Adapted from Welander (1986).
- 14 Having said this, Bryan (1986), Manabe & Stouffer (1988) and Marotzke (1989) did find evidence of multiple equilibria in various three-dimensional numerical models, motivated in part by the solutions of box models.
- 15 After Stommel *et al.* (1958).
- 16 Following Stommel & Arons (1960).
- 17 A global Stommel–Arons-like solution was presented by Stommel (1958). The discovery of deep western boundary currents by Swallow & Worthington (1961) was motivated by the theoretical model. Using neutrally-buoyant floats underneath the Gulf Stream they found an equatorward-flowing undercurrent with typical speeds of $10\text{--}20\text{ cm s}^{-1}$. Some relevant observations of the deep circulation are summarized by Hogg (2001).
- 18 For example, Toggweiler & Samuels (1995).
- 19 Drawing from the various numerical, conceptual and analytic models of Toggweiler & Samuels (1995, 1998), Döös & Coward (1997), Gnanadesikan (1999), Vallis (2000), Webb & Sugino (2001), Nof (2003), Samelson (1999a, 2004), Wolfe & Cessi (2011), and Nikurashin & Vallis (2011, 2012). The notion of a deep interhemispheric circulation driven by winds in the ACC was earlier proposed by Eady (1957), albeit rather sketchily. None of our models of the MOC (including the ones in later sections) are complete, never mind true, but some may be useful.
- 20 Loic Jullion graciously provided the inverse calculations, which are similar to those described in Lumpkin & Speer (2007). Patrick Heimbach kindly provided the state estimates, which are from the ECCO suite of calculations.
- 21 From Rintoul *et al.* (2001).
- 22 See Rintoul *et al.* (2001) and Olbers *et al.* (2004) for ACC reviews.
- 23 These simulations, described in Henning & Vallis (2005), solve the primitive equations in a domain similar to Fig. 21.19. The wind forcing produces a poleward Ekman drift across the channel, as well as a subtropical gyre, and there is a meridional temperature gradient across the whole domain, so giving rise to a subtropical thermocline.
- 24 Adapted from Henning & Vallis (2005).
- 25 Munk & Palmén (1951), Gille (1997) and Stevens & Ivchenko (1997).
- 26 Adapted from a figure in Burke *et al.* (2015).
- 27 Models of this ilk stem from Johnson & Bryden (1989), Straub (1993), Hallberg & Gnanadesikan (2001) Karsten *et al.* (2002), Marshall & Radko (2003), Henning & Vallis (2005), consider related issues and extensions.
- 28 See also Munk & Palmén (1951), Warren *et al.* (1996), Olbers (1998) and Hughes (2002).
- 29 Similar to a figure in Watson *et al.* (2015).
- 30 Largely following Nikurashin & Vallis (2011, 2012). For related numerical simulations see Vallis (2000) and Wolfe & Cessi (2010, 2011).
- 31 A full description may be found in Nikurashin & Vallis (2012). In the form described here the model becomes similar to the one of Gnanadesikan (1999).
- 32 A continuous, unique, pole-to-pole isoneutral pathway is a chimera, because of the nonlinear dependence of density on pressure, temperature and salinity in the seawater equation of state. But at the level of our theory there is an approximate one. See also endnote 9 on page 53.
- 33 For variations involving multiple basins see Ferrari *et al.* (2014) and Thompson *et al.* (2016).

